## Title

Revelations about tropical cyclones from A-train satellite data: the effect of environmental aerosols on tropical cyclone formation, and the origin of ozone in the eyes of mature tropical cyclones



## Author

COLLIMORE, CHRISTOPHER CRAIG

## Publication Date

2018

Peer reviewed|Thesis/dissertation

UNIVERSITY OF CALIFORNIA

Los Angeles

# Revelations About Tropical Cyclones from A-Train Satellite Data: the Effect of Environmental Aerosols on Tropical Cyclone Formation, and the Origin of Ozone in the Eyes of Mature Tropical Cyclones

A dissertation submitted in partial satisfaction of the

requirements for the degree Doctor of Philosophy

in Atmospheric and Oceanic Sciences

by

Christopher Craig Collimore

2018

ABRSTRACT OF THE DISSERTATION

Revelations About Tropical Cyclones from A-Train Satellite Data: the Effect of Environmental Aerosols on Tropical Cyclone Formation, and the Origin of Ozone in the Eyes of Mature Tropical Cyclones

by

Christopher Craig Collimore

Doctor of Philosophy in Atmospheric and Oceanic Sciences

University of California, Los Angeles, 2018

Professor Robert G. Fovell, Chair

Prior studies have shown that high levels of aerosols in the environment of convective clouds can cause the convection to become more vigorous through a five step process. Tropical cyclones (TCs) start as clusters of convective clouds; intense convection is important for the development of the cluster into a TC. This study tests the hypothesis that high aerosol content in the vicinity of a convective cloud cluster increases the chances that the cluster will develop into a TC by invigorating its convection. This study centers on 63 clusters that developed into TCs (developers) and 98 clusters that dissipated before becoming a TC (nondevelopers). Using observations from a satellite associated with the "A-train" group of satellites, it was established that the average aerosol content surrounding developers was significantly higher than that

surrounding nondevelopers. Furthermore, A-train measurements were used to establish that each of the five steps associated with invigoration of convection by aerosols were more prominent in the developers than in the nondevelopers. Altogether, the data suggests convective cloud clusters embedded in regions with elevated aerosols may have a greater likelihood of developing into a TC because the aerosols may invigorate their convection.

A-train satellite data are also used to investigate ozone levels in the eyes of mature TCs. Several previous studies have found evidence of high ozone levels inside TC eyes. Explanations for the elevated ozone involve intrusion of ozone-rich stratospheric air downward into the eye or a lower tropopause over the eye. Other studies have found no evidence of elevated ozone in TC eyes. However, ozone measurements from both types of studies (evidence and no evidence of elevated ozone) were less than optimal. This study analyses seven mature TCs with satellite overpasses directly over the eye – an optimal situation for ozone measurement. The results indicate TCs can have very high ozone concentrations in the eyewall. This suggests eyewall lighting produces the ozone. The data also suggest the elevated ozone content in the eyewall is often transported into the eye. Thus TC eyes can contain elevated ozone levels, but the source appears to be the eyewall, not the stratosphere.

The dissertation of Christopher Craig Collimore is approved:

Jasper F. Kok

Donald N. Ylvisaker

Jochen Peter Stutz

Eric Fetzer

Robert G. Fovell, Committee Chair

University of California, Los Angeles

2018

# DEDICATION

Dedicated to

Eric Fetzer and Bill Gray

The two greatest advisors ever

## TABLE OF CONTENTS

LIST OF FIGURES

LIST OF TABLES

ACKNOWLEDGEMENTS

Figure 3.8 is reprinted from Zou, X. and Y. Wu, 2005: On the Relationship Between Total Ozone Mapping Spectrometer (TOMS) Ozone and Hurricanes. *J. Geophys. Res.*, **110**, D06109, doi:10.1029/2004JD005019

Chapters 2 and 3 are manuscripts in preparation for publication to be co-authored with Eric J. Fetzer and Robert G. Fovell. I would like to thank both co-authors for their advice and beneficial discussions on various topics related to processing data, interpreting results, and conveying the results clearly in the manuscripts.

I am grateful to Joe Turk for providing data essential for the analyses in Chapter 3, to Donald N. Ylvisaker for providing guidance related to the statistics used in Chapter 3, and to the World Wide Lightning Location Network (http://wwlln.net), a collaboration among over 50 universities and institutions, for providing the lightning location data used in Chapter 3.

This work was supported by The NASA Hurricane Science Research (HSRP) Program, the NASA Energy and Water-cycle Study (NEWS) Program, and the NASA Making Earth System Data Records for Use in Research Environments (MEaSUREs) Program.

I would also like to thank Jochen Stutz, Jasper Kok, Kristen Corbosiero, Dan Brown, Brian Kahn, Robert Holzworth, David Haffner, and Thomas Kurosu for their help with this study. Finally, I would like to thank Eric J. Fetzer and Robert G. Fovell for their advice, support, patience, friendship, and many discussions that shaped this work.

Christopher Craig Collimore

Los Angeles, California

May, 2018

## CHRISTOPHER CRAIG COLLIMORE

**Education**

| | | |
|---|---|---|
| B.A., Geography | 1985 | Dartmouth College (cum laude) |
| M.S., Atmospheric Science | 1989 | Colorado State University (with thesis) |
| | | Advisor: Dr. William M. Gray |

**Selected Work Experience (University of Wisconsin-Madison: Space Science and Engineering Center and Dept. of Atmospheric and Oceanic Sciences)**

| | |
|---|---|
| 2000-2003 | Regional Modulation of Tropical Deep Convection by the Quasi-Biennial Oscillation. NSF project; Co-Principal Investigator |
| 1998-2000 | A Study of Tropical Deep Convection at Quasi-Biennial and Annual Time Scales. NSF project; Co-Principal Investigator |
| 1997-1998 | An Investigation of the Low-level Temperature Inversion Over Antarctica Using Satellite Data. Internal Space Science and Engineering Center Project, U. of Wisconsin-Madison; Researcher |
| 1996-1997 | Multi-Satellite Estimates of Land-Surface Properties for Determination of Energy and Water Budgets. NASA project; Researcher |
| 1994-1996 | Satellite-Based Remote Sensing of Tropical Cyclones. Naval Research Laboratory project; Researcher |
| 1991-1994 | Investigation of Cloud Properties, Atmospheric Stability and Total Ozone with MODIS. NASA project; Researcher. |

**Selected Publications**

Collimore, C. C., D. W. Martin, M. H. Hitchman, A. Huesmann and D. E. Waliser, 2003:

On the Relationship Between the QBO and Tropical Deep Convection. *J. Climate,* **16**, 2552-2568.

Collimore, C. C., M. H. Hitchman and D. W. Martin, 1998: Is There a Quasi-Biennial Oscillation in Tropical Deep Convection? *Geophys. Res. Letters,* 25, 333-336.

Collimore, C. C., 1990: Associations between West Pacific equatorial zonal winds and East Pacific SST anomalies. Department of Atmospheric Science, Colorado State University, Paper No. 468, 103 pages.

Rabin, R. M., B. A. Burns, C. Collimore, G. R. Diak and W. Raymond, 2000: Relating Remotely-Sensed Vegetation and Soil Moisture Indices to Surface Energy Fluxes in Vicinity of an Atmospheric Dryline. *Remote Sensing Reviews,* 18, 53-82.

Smith, W. L., S. A. Ackerman, H. Chung, C. Collimore, R. A. Frey, L. Herman, F. Nagel, H. Revercomb, H. Woolf, F. Wu and D. Zaras, 1993: Final report of NASA contract NAS1-18272: ERBE scientific investigations. Cooperative Institute for Meteorological Satellite Studies, Space Science and Engineering Center, Madison, WI, SSEC Publication No. 93.12.S1.

**Selected Conference Proceedings and Presentations**

Collimore, C. C., D. E. Waliser, G. L. Smith, T. D. Bess, D. F. Young, D. W. Martin and K. A. Bush, 2001: An Alternative Long Term OLR Data Set. AMS 11th Conference on Satellite Meteorology and Oceanography, 15-18 October, Madison, Wisconsin.

Collimore, C. C., D. W. Martin, M. H. Hitchman and A. Huesmann, 2000: The Influence of the QBO on Tropical Deep Convection. 24$^{th}$ Conference on Hurricanes and Tropical Meteorology, 29 May – 2 June, Ft. Lauderdale, Florida.

# CHAPTER 1

## Introduction

The A-train is a group of six satellites that follow one another, single file, through the same orbit. The orbit is a sun-synchronous, polar orbit. They pass through the same point as little as a few seconds apart. Most of the satellites carry several instruments. Thus, numerous parameters can be measured for the same place on Earth at nearly the same moment in time. A-train observations contain a wealth of information for TCs that has yet to be utilized for scientific research. This study aims to take advantage of the large quantity and excellent quality of A-train observations to demonstrate how useful A-train measurements can be for studying TCs from their genesis to their peak intensity while, at the same time, unveiling new insights into TC formation and TC dynamics during the mature stage of the TC lifecycle.

Chapter 2 describes an examination of the relationship between TC formation and aerosol content in the environment of convective cloud clusters before they have developed into TCs. Data from an A-train satellite and from the Terra satellite are used to show that high aerosol content in the vicinity of a tropical cloud cluster may increase the likelihood that the cluster will evolve into a TC (Terra complements the A-train satellite named Aqua – both carry two of the same instruments, but Terra has a local time of overpass in the morning and Aqua has a local time of overpass in the afternoon). A-train/Terra measurements provide evidence that high aerosol content invigorates convection within a cluster and that the enhanced convection spurs the development of the cluster into a TC. The results have important implications for the prediction of TC formation.

Chapter 3 describes an investigation into the presence of high ozone concentrations inside TC eyes. Observations from a third instrument on board a third A-train satellite are used to show

that a TC eye can contain very high levels of ozone. The results suggest a different source of the ozone than that proposed in previous studies and they explain why ozone is sometimes observed, and sometimes not observed, in TC eyes. Furthermore, the findings lend insight into the dynamics of the eye and eyewall in a TC and have possible implications for the prediction of TC intensity.

# CHAPTER 2

## The Effect of Environmental Aerosols on Tropical Cyclone Formation

### 2.1 Introduction

Enhancement of tropical convection by high concentrations of aerosols has been well established. Several studies have found that when convective clouds form in regions of anomalously high aerosol concentrations, the increased number of cloud condensation nuclei (CCN) results in clouds with more, and thus smaller, cloud droplets compared to clouds that form in regions with lower aerosol concentrations. The smaller droplets weigh less and therefore can be lofted to higher altitudes by convective updrafts. As a result, more droplets reach altitudes where they can freeze. The extra latent heat released upon freezing creates increased buoyancy which induces stronger updrafts -- more vigorous convection (Tao et al. 2007; Rosenfeld et al. 2008; Lynn and Khain 2010; Krall and Cotton 2012; Rosenfeld et al. 2012). Vigorous convection is critical for the tropical cyclone (TC) formation process. TCs start as simple cloud clusters comprised almost entirely of convective clouds and products of convective clouds, such as cirrus. The convection fuels a circulation which becomes increasingly organized and increasingly similar to that of a TC until finally the cluster becomes a TC (Gray 1998, Hendricks et al. 2004). This study tests whether or not high aerosol concentrations in the environment of a convective

cluster increase the likelihood that the cluster will develop into a TC by enhancing convection within the cluster.

## 2.2 Methodology and Data

### 2.2.1 *Methodology*

Our overall strategy was to collect satellite observations of atmospheric parameters relevant to the effect high aerosol concentrations have on convection, then average them for cloud clusters in the Atlantic; averages for clusters that develop into TCs (developers) were then compared to averages for clusters that do not develop into TCs (nondevelopers). If developer parameters are more consistent with the invigoration of convection by aerosols, that would suggest aerosol invigoration usually plays a role in TC formation. The relevant parameters are aerosol content in the environment surrounding cloud clusters, and cloud particle size, cloud top pressure, ice cloud amount, and latent heat release within the clusters.

For a given cloud cluster, we collected daily aerosol content observations in and surrounding it over its lifetime (from the time corresponding to the first observations of the cluster until it either dissipated or became a TC), then created composite means of those observations relative to storm center. Then we averaged the composite means for all of the developers to produce mean aerosol content in and near developers, and did the same for nondevelopers. Developer and nondeveloper means for all of the other parameters were created in the same manner except for the ice cloud percentages of Section 2.3.4 which were created in a slightly different manner (this manner is described in Section 2.3.4).

### **2.2.2** *Cloud Cluster Data*

Throughout the year, the National Hurricane Center (NHC) monitors cloud clusters in the Atlantic and identifies any that show promise of developing into a TC. Their assessment relies partly on environment conditions. NHC opens an *investigation* on any clusters that show promise of development, so those clusters are called *invests*. We examined only invests identified by NHC.

In order to composite satellite observations on a storm's center, information on storm center location is needed. We obtained center location information from NHC's "best tracks". After opening an investigation on an invest, NHC tracks the location of the center and measures other aspects of the invest operationally. When the hurricane season ends, NHC has the time to re-assess the center locations (and other aspects) more carefully using all available data. The information in these "best tracks" is more accurate than that in the operational tracks. We examined the invests NHC identified over a four year span: 2005 to 2008. During this period, NHC identified 161 invests: 63 developers and 98 nondevelopers. After being declared an invest, these 161 invests lasted one to ten days (roughly two days on average) before either becoming a TC or beginning to dissipate.

### **2.2.3** *Aerosol and Cloud Property Data*

We obtained aerosol content, cloud particle size, and ice cloud amount data from the Moderate Resolution Imaging Spectroradiometer (MODIS) on board the Terra satellite (version 6 of the three data products). Terra, a polar-orbiter, passed over each cloud cluster twice a day -- once during daylight, once at night. MODIS requires sunlight to measure the three parameters we obtained, so only the daytime overpasses were of use. Terra is sun-synchronous with a local time

of overpass of around 10:30 am during the day. The horizontal resolution of the aerosol measurements is 1 km, but the measurements are binned together to produce a data set at 10 km resolution (at nadir). The resolution of the cloud property data is 1 km, but we chose to use a dataset subsampled at 5 km resolution – only one measurement out of every 5 by 5 km box (at nadir) is included.

We obtained temperature, relative humidity, and cloud top pressure data from the Atmospheric Infrared Sounder (AIRS) on board the Aqua satellite (version 6 of the three data products). For consistency with the data from Terra, we only used daytime AIRS data. Aqua is also a sun-synchronous polar-orbiter but with a local time of overpass near 1:30 pm during daylight hours. The resolution of AIRS data is about 45 km at nadir. AIRS data incorporates microwave observations from the Advanced Microwave Sounding Unit (AMSU, also on Aqua) in order to measure temperature and humidity throughout the inside of clouds.

### 2.3 Parameters related to convective invigoration by aerosols: developer vs. nondeveloper comparisons

#### 2.3.1 *Environmental Aerosol Content*

MODIS measures aerosol content as aerosol optical depth (AOD). MODIS AOD measurements are for the entire atmosphere, but most aerosols are in the troposphere (Seinfeld and Pandis 2006), so most of the signal in the AOD measurements will be from the troposphere – where hurricanes exist. More aerosols result in higher values of AOD. Figure 2.1 shows mean developer AOD minus mean nondeveloper AOD. There are fewer observations in the eastern third of Fig. 2.1 because sunglint interferes with MODIS AOD measurements. The white circle represents a typical size for a cloud cluster (about 700 km diameter, Gray 1998). It may seem

surprising to see AOD observations inside the white circle since MODIS AOD can only be measured for clear locations. However, clusters often have clouds that are asymmetric about the center of the cluster's low level circulation (which is defined as the cluster's center) and clear areas occupying the rest of the circulation.

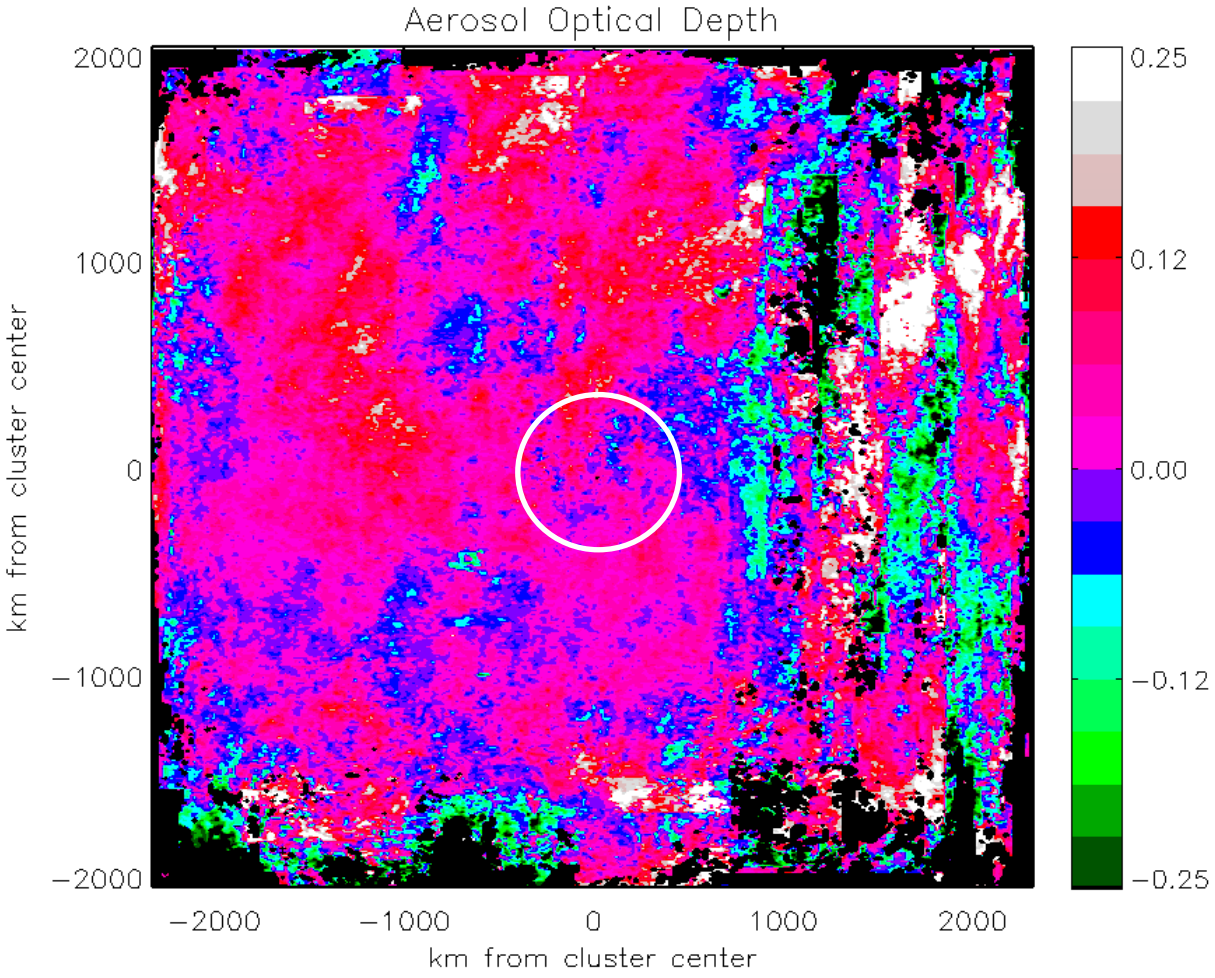


Figure 2.1: Composite mean AOD in and surrounding developers minus the same for nondevelopers. The white circle at the center represents a typical size for developers and nondevelopers. AOD is unitless.

The vast majority of the environment surrounding developers has AOD that is substantially higher than the AOD in the environment surrounding nondevelopers. In many areas

developer means are at least 0.10 higher than nondeveloper means – quite a large difference. As noted above, MODIS cannot measure AOD for locations with clouds. However, the aerosol content within the developer and nondeveloper cloud clusters should be roughly the same as the content in the nearby environment – the clusters would have drawn in ambient aerosol concentrations with their low-level inflow. This is true whether the clusters formed inside regions with the measured aerosol characteristics or migrated into those regions after forming.

Neither type of cloud cluster is likely to encounter aerosols in the extended environment shown in Fig. 2.1. Therefore we focus on a box centered on storm center, 1200 km on a side. This box approximates the area containing aerosols close enough to the clusters to be advected into the clusters with the low-level inflow. For developers, AOD averaged inside the box is 0.245, for nondevelopers it is 0.197 (see Table 2.1). Thus, AOD in and near developers is 24% higher than AOD in and near nondevelopers. The difference between developer and nondeveloper mean AOD is significant at the 99% level using Student's t test.

Note: for the statistical significance of the developer minus nondeveloper difference for other parameters discussed below, refer to Table 2.1. The sample sizes in Table 2.1 do not match the number of developers and nondevelopers we studied (63 and 98, respectively) because problems with measurements sometimes resulted in not enough observations to make reliable means.

### **2.3.2** *Cloud Particle Size*

In the first step of invigoration of convection by aerosols (discussed in Section 2.1), ingestion of high aerosol content by convective clouds leads to more numerous, and thus smaller, cloud particles. Accordingly, the higher aerosol content in the vicinity of developers should

cause their cloud particles to be smaller than nondeveloper cloud particles. Therefore, we now compare cloud particle size in developers and nondevelopers.

Table 2.1: Parameters, for developers and nondevelopers, related to invigoration of convection by aerosols. AOD was averaged over a box centered on storm center, 1200 km on each side. Cloud particle radius, cloud top pressure, and ice cloud percentage were averaged over a similar box, 400 km on each side. Temperature, a proxy for latent heating, was averaged from storm center to a radius of 250 km and between 500 and 250 hPa. Units for the means and standard deviations: microns for cloud particle radius, hPa for cloud top pressure, and K for the latent heating proxy. AOD is unitless. Sample size refers to the number of developers or nondevelopers. A positive percent difference means developer values are larger. Significance refers to the probability that the difference between means did not occur by chance, as determined by Student's t test. The (-13) next to the percent difference for cloud particle radius refers to the corresponding percent difference in cloud particle volume.

| | Mean | Standard Deviation | Sample size | Percent Difference Between Means | Significance (%) |
|---|---|---|---|---|---|
| AOD | | | | 24 | 99 |
| Developers | 0.245 | 0.103 | 56 | | |
| Nondevelopers | 0.197 | 0.084 | 89 | | |
| Cloud Particle Radius | | | | -4 (-13) | 95 |
| Developers | 26.3 | 2.55 | 57 | | |
| Nondevelopers | 27.4 | 3.67 | 90 | | |
| Cloud Top Pressure | | | | -17 | 99.9 |
| Developers | 200 | 27 | 53 | | |
| Nondevelopers | 233 | 48 | 87 | | |
| Ice Cloud Percentage | | | | 11 | 99 |
| Developers | 81 | 12 | 57 | | |
| Nondevelopers | 73 | 19 | 90 | | |
| Latent Heating Proxy | | | | 118 | 99.9 |
| Developers | 1.48 | 0.87 | 55 | | |
| Nondevelopers | 0.68 | 3.15 | 89 | | |

Cloud particle size depends partly on cloud particle phase (ice or liquid). When determining the size and phase of particles in a convective cloud, MODIS uses information primarily from the top portion of the cloud (Platnick 2000; van Diedenhoven 2016). Thus in the discussion to follow, a convective cloud with liquid droplets at low altitudes but an upper portion comprised of ice crystals is considered an ice cloud. Of course cirrus clouds are ice clouds too.

Ice crystals tend to be larger than liquid droplets (Chang-Hoi et al. 1998; Shupe et al. 2001; Daniel Cziczo, personal communication 2017). So a comparison of ice clouds and liquid clouds cannot distinguish whether particle size differences between the two are due to the influence of aerosols or particle phase. Developers and nondevelopers have different ratios of ice clouds to liquid clouds (see next section). Therefore, it is important to examine clouds of the same phase when comparing particle sizes in the two types of cloud clusters. We examine ice clouds and we do so for several reasons, three of which are: 1) most clouds in both types of cloud clusters are ice clouds; 2) the ice formation process, and thus ice clouds, are central to the mechanisms we are investigating, as discussed earlier in Section 2.1; 3) we are most concerned with convective clouds, and in the tropical cloud clusters we are investigating, ice clouds are almost certainly convective in origin (e.g., convection or cirrus produced by convection), whereas liquid clouds have a greater likelihood of being nonconvective in origin (such as low stratus).

The MODIS instrument estimates the effective radius of cloud particles. MODIS produces four separate effective radius products, each utilizing different wavelengths of sunlight reflected by cloud particles. Retrievals for all four products often fail when MODIS views cirrus clouds, but retrievals for the *Cloud_Effective_Radius_37* product fail less frequently than the

others (Gala Wind, personal communication 2017). Since the cloud canopies of the cloud clusters we are analyzing are mostly comprised of cirrus, and for other reasons, we concluded that *Cloud_Effective_Radius_37* is the most appropriate product to use in our analyses of cloud particle size.

Figure 2.2 shows mean *Cloud_Effective_Radius_37* for ice clouds in developers minus the same quantity in nondevelopers. Developers generally have smaller effective radii. This is

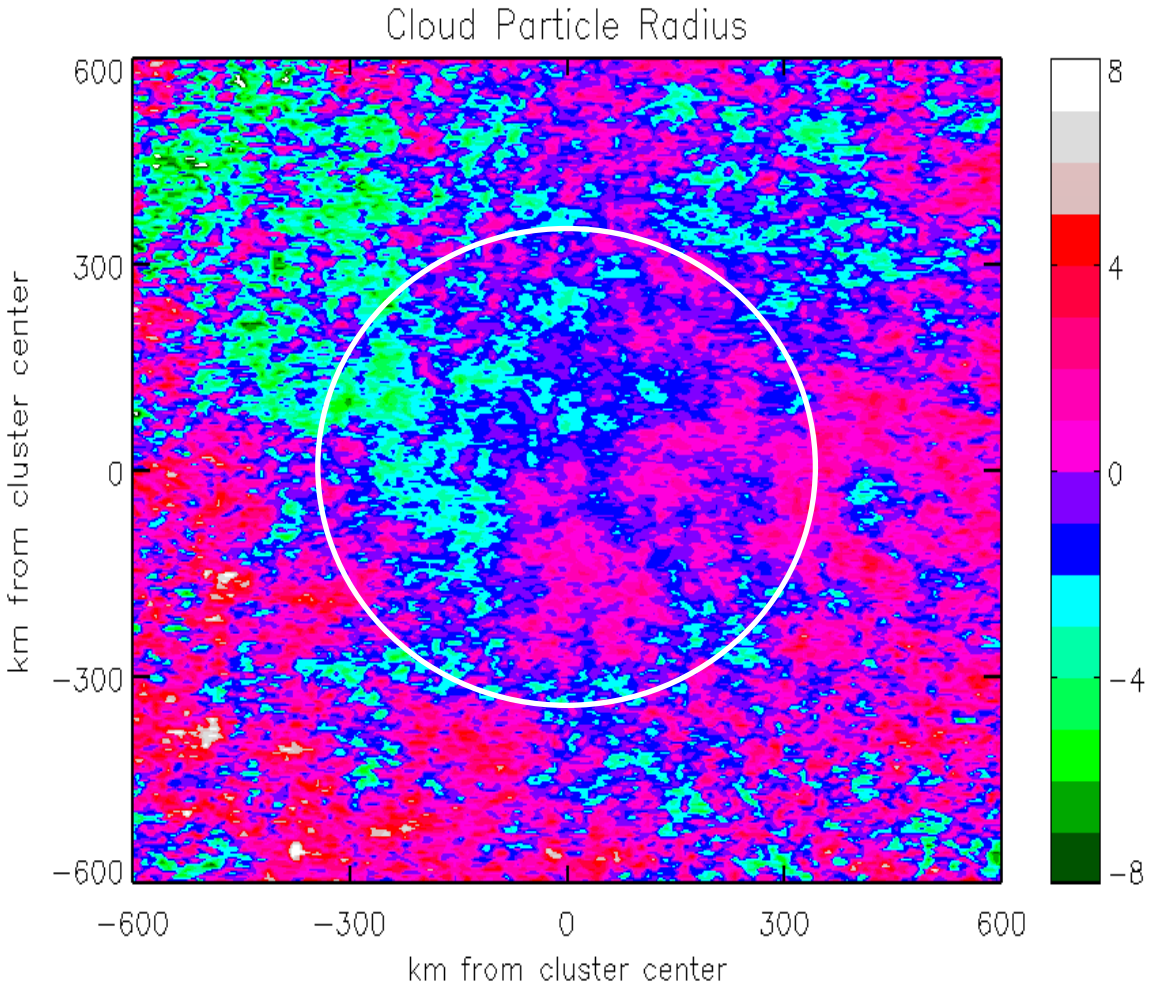


Figure 2.2: Composite mean of cloud particle effective radius in developers minus the same for nondevelopers. The white circle represents a typical size for developers and nondevelopers. Units are microns.

consistent with ingestion of more aerosols, as suggested by Fig. 2.1. In regard to particle size, we are only concerned with measurements inside the cloud clusters and not the nearby environment. So now we focus on a smaller box than that used for the AOD means. We averaged data inside a box 400 km on a side, centered on storm center. This box should only include data inside the cloud clusters . For developers, mean effective radius inside this box is 26.3 microns, while for nondevelopers it is 27.4 microns (Table 2.1). Thus developer cloud particles are over 4% smaller than nondeveloper particles. This may not seem like a big difference, but it roughly equates to a 13% difference in mean particle volume [assuming most ice crystals have shapes with volumes roughly proportional to the radius cubed (liquid drops often remain roughly spherical after freezing; Järvinen, et al. 2016; Schmitt et al. 2016) and assuming developers and nondevelopers have a similar mixture of ice crystal shapes]. Particle volume is more important for the processes we are investigating than is particle radius (particle volume is more relevant to particle weight; see Section 2.1 or the next section for the importance of particle weight).

### **2.3.3** *Cloud Top Pressure*

In the second step of convective invigoration by aerosols, convective updrafts carry smaller (and thus lighter) cloud particles to higher altitudes. Accordingly, the small size of developer particles relative to nondeveloper particles should lead to developer clouds that are taller than nondeveloper clouds. Figure 2.3 shows mean cloud top pressure in developers minus that in nondevelopers. Only clouds taller than 500 hPa are included in the means (and no clear scenes are included). Throughout most of the area occupied by the cloud clusters, pressures are lower in developers indicating, as expected, taller clouds.

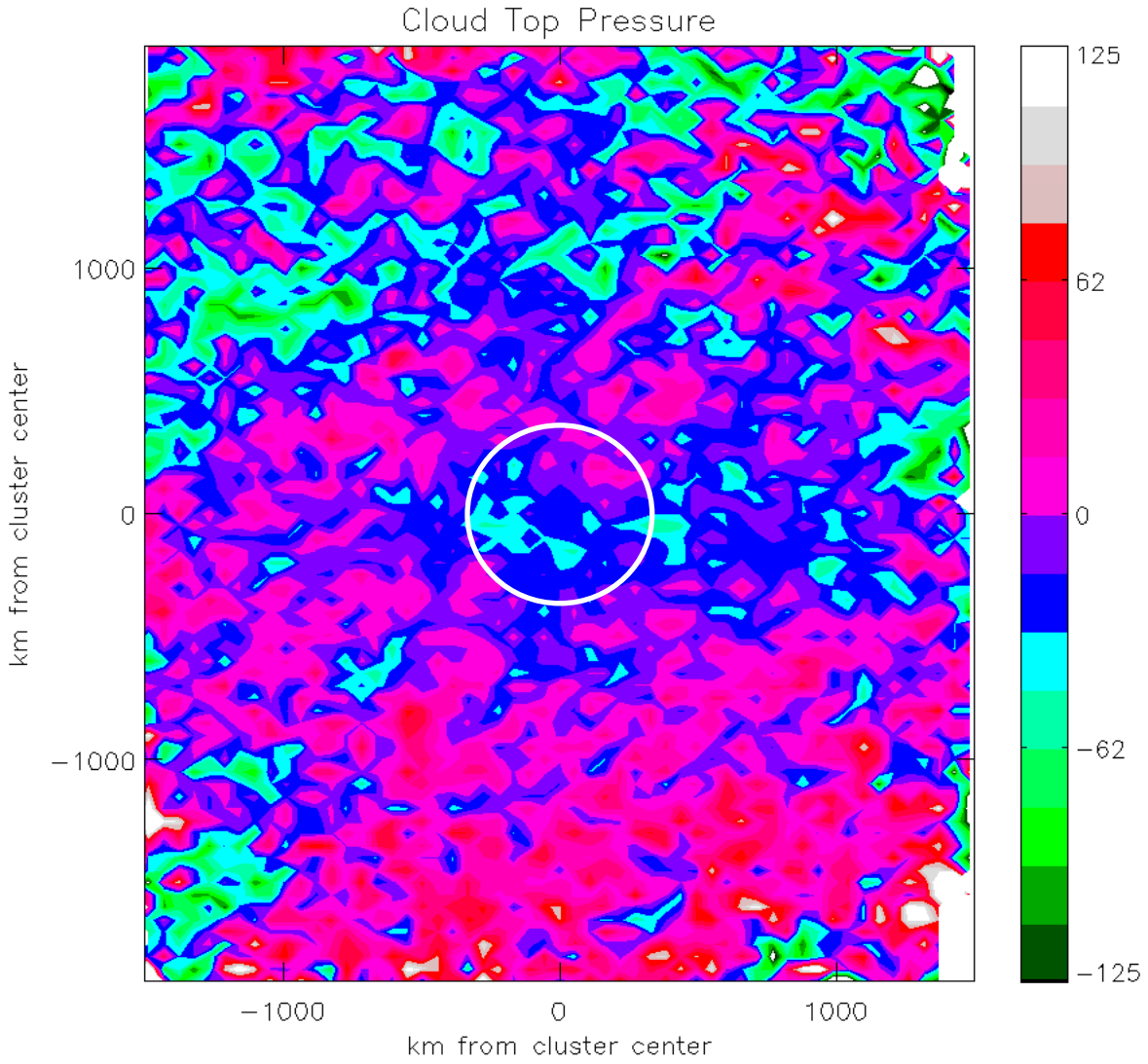


Figure 2.3: Composite mean of cloud top pressure in developers minus the same for nondevelopers. The white circle represents a typical size for developers and nondevelopers. Units are hPa.

The negative values emanating from the clusters toward the east and, to a lesser extent, the west (indicating lower cloud top pressures outside developers) are consistent with more and/or higher cirrus cloud outflow from the developers. The areas to the east and west may have contained cirrus from developers and convection with lower cloud tops from nondevelopers, or

perhaps cirrus from developers and cirrus at lower altitudes from nondevelopers. The developers and nondevelopers of this study are from a range of latitudes in the tropics and subtropics of the Atlantic. The upper level winds throughout this region are primarily zonal and thus cirrus outflow from the clusters should mostly be aligned in the east-west direction. Therefore, if developers did indeed have more/higher cirrus outflow, the resultant impacts on developer minus nondeveloper cloud top pressure in the environment would be mainly to the east and west, as is seen in Fig. 2.3.

Mean cloud top pressure in developers (inside a 400 km box centered on storm center) is 200 hPa. For nondevelopers, this quantity is 233 hPa. Thus developer cloud tops are 17% higher than nondeveloper cloud tops (Table 2.1).

### **2.3.4** *Ice Clouds*

In the third step of convective invigoration by aerosols, cloud droplets freeze after reaching higher, colder altitudes. Since developers have taller clouds than nondevelopers, they should have more ice clouds than nondevelopers. Figure 2.4 shows the percentage of developer clouds that are ice clouds minus the percentage of nondeveloper clouds that are ice clouds. As expected, developers generally have more ice clouds than nondevelopers. The mean percentage of ice clouds inside the developer 400 km box is 81%, while the nondeveloper mean percentage is only 73% (Table 2.1; for the lifetime of each cluster, the number of ice cloud observations in the box was totaled and then divided by the number of cloud observations in the box; these percentages were then averaged for developers and for nondevelopers). Thus, the presence of ice clouds is 11% higher in developers [the percent difference in ice cloud percent is 11%: $(P_d - P_n)/P_n$ where $P_d$ = developer percentage and $P_n$ = nondeveloper percentage].

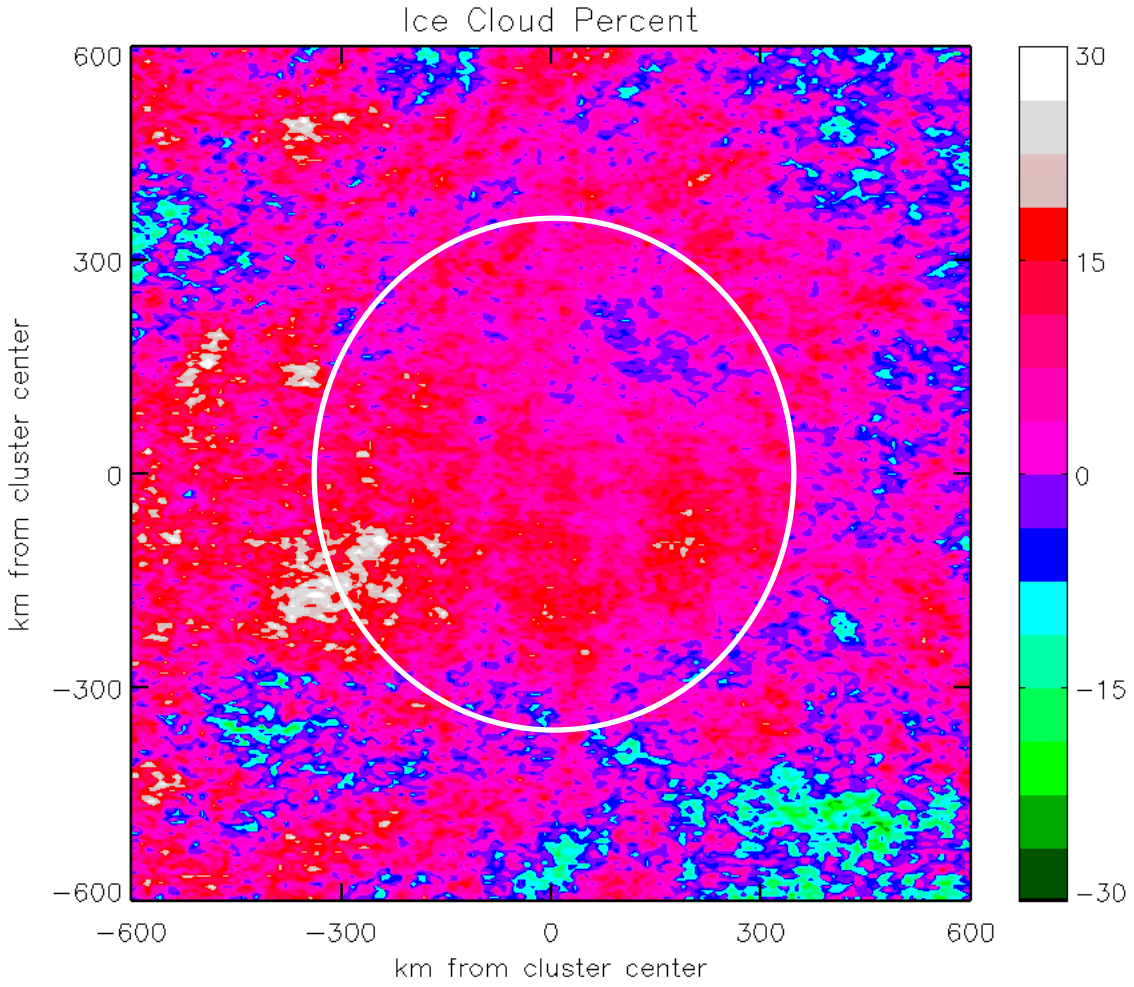


Figure 2.4: Percentage of clouds that were ice clouds in developers minus the same for nondevelopers. The white circle represents a typical size for developers and nondevelopers.

### **2.3.5** *Latent Heat Release*

In the fourth step of convective invigoration by aerosols, latent heat is released as droplets freeze. Since developers have more ice clouds than nondevelopers, they should have more latent heat release. Figure 2.5 shows the mean vertical structure of temperature in developers, azimuthally averaged for different radii from storm center, minus the same for

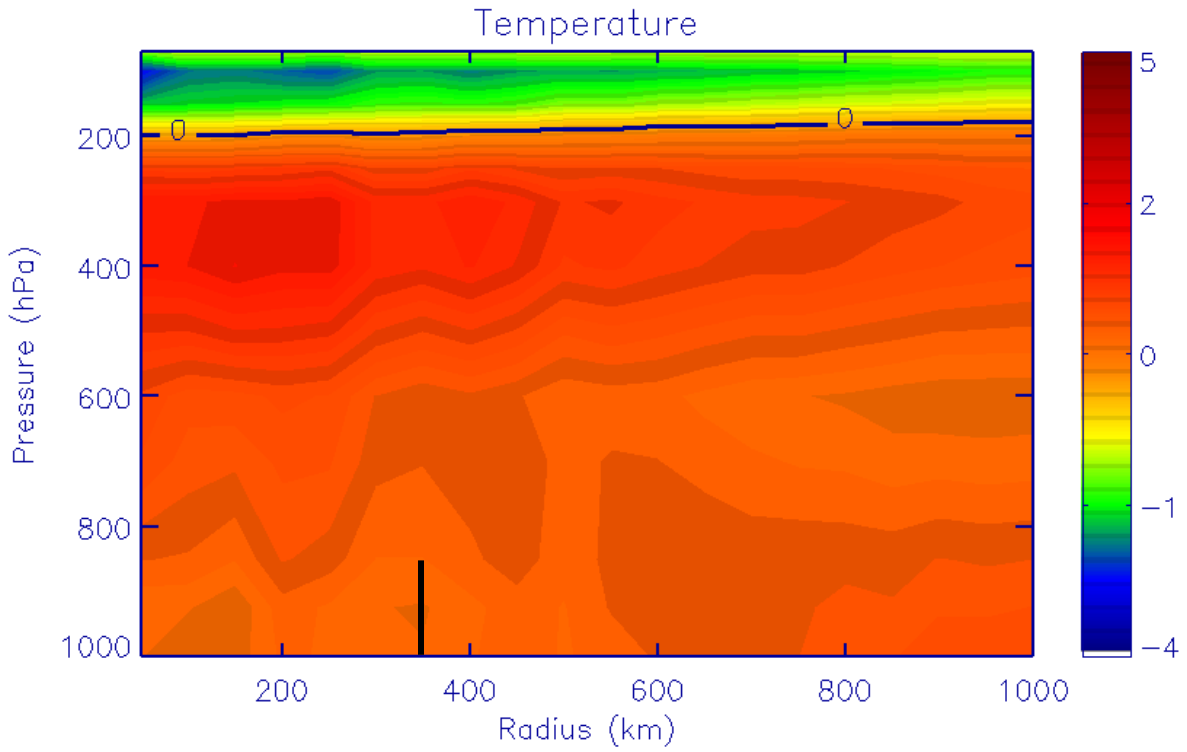


Figure 2.5: Azimuthal mean temperature in and near developers minus that for nondevelopers as a function of height and radius from storm center.

nondevelopers. The typical outer edge of both types of cloud clusters – a radius of 350 km – is indicated by the vertical line near the bottom of the plot. The freezing level in the tropical North Atlantic is usually close to 600 hPa (Dunion 2011). Developers have higher temperatures between 600 hPa and the tropopause (roughly 240 hPa), consistent with more latent heat release from freezing in developers. (The colder temperatures above 240 hPa are most likely due to a higher tropopause over the developers as a result of the deeper convection discussed earlier).

Next, we quantify and compare the latent heat release in developers and nondevelopers. In regard to temperatures inside cloud clusters that are above environmental values at the same altitude, we assume the temperature difference is due to latent heat release and use that

difference as a proxy for latent heat release. To represent temperatures inside clusters, we calculated the mean value between 500 and 250 hPa and from the center to a radius of 250 km. For environmental temperatures, we averaged values at the same pressure levels but between radii of 850 and 1000 km. The mean latent heating (i.e., the difference between temperature inside clusters and temperature in the environment) is 1.48 °C for developers and 0.68 °C for nondevelopers (Table 2.1). Thus latent heating in developers is 118% larger than that in nondevelopers. This difference is quite high and may be partially due to the final step of convective invigoration by aerosols. In the final step, the extra latent heat release from freezing and concomitant increase in buoyancy causes stronger updrafts – more intense convection. The much higher latent heating in developers may be partially due to more condensation (vapor to liquid above the freezing altitude) and more freezing (more droplets carried to high, cold altitudes) as a result of this enhanced convection.

## 2.4 Discussion

As Fig. 2.1 illustrates, developers are typically immersed in aerosol concentrations that are significantly higher than those for nondevelopers, suggesting that convective cloud clusters surrounded by elevated aerosol levels have a substantially higher chance of developing into TCs compared to clusters surrounded by lower aerosol concentrations. This alone is notable. The rest of our results illustrate a likely mechanism through which the high aerosol concentrations may have contributed to the evolution of the developers into TCs – invigoration of convection.

Our results are consistent with each step of the invigoration process. The first step is for enhanced aerosol loading to provide convective clouds with more cloud condensation nuclei, resulting in clouds with more numerous – and thus smaller – cloud droplets compared to clouds

exposed to lower aerosol conditions. Consistent with this, developers typically have smaller cloud particles than nondevelopers (Fig. 2.2). The next step is for many of the smaller, and thus lighter, droplets to be lofted to higher altitudes. On average, developer cloud tops are indeed higher in altitude than nondeveloper cloud tops (Fig. 2.3). Next, the droplets which have reached higher, colder altitudes freeze. In line with this step, ice clouds comprise a higher percentage of the clouds in developers compared to nondevelopers (Fig. 2.4). Next, as the droplets freeze, latent heat is released. Correspondingly, the upper levels of developers are warmer than those for nondevelopers (Fig. 2.5).

Finally, the extra latent heat released upon freezing creates increased buoyancy which induces stronger updrafts – i.e., more intense convection. It is not possible to measure updrafts with satellite instruments, but the more prominent cirrus outflow from developers (see Section 2.3.3) is indirect evidence of stronger updrafts. Furthermore, the taller clouds in developers (Fig. 2.3) may also be evidence of stronger convection: in addition to being a result of smaller, lighter cloud particles, the taller clouds may be partially due to stronger updrafts. Moreover, as discussed in Section 2.3.5, the large amount of latent heating in developers relative to that in nondevelopers may be partially due to stronger convection. These three indicators of stronger convection in the developers (more prominent cirrus outflow, taller clouds, and greater latent heating) suggest that the developers had more intense convection than the nondevelopers.

The evidence of all five steps of the aerosol invigoration process that developers display suggests that the elevated aerosol content surrounding developers may have invigorated their convection. There are several theories for TC formation, but convection is at the heart of all of them. Therefore, the elevated aerosol content surrounding the developers may have facilitated their transition into TCs by invigorating their convection.

However, in addition to ambient aerosol loading, several other environmental factors could have been important for the taller clouds (Fig. 2.3), more prevalent ice clouds (Fig. 2.4), greater latent heating (Fig. 2.5), and more intense convection (see previous paragraph) developers had compared to nondevelopers. Humidity is one such environmental factor. As Fig. 2.6 shows, the relative humidity (RH) in developer environments was higher than the RH in nondeveloper environments (a corresponding plot of water vapor mixing ratio looks very similar, see Fig. 2.8). The higher RH most likely facilitated the larger values of all four parameters (the higher RH would have enhanced developer cloud height directly, then ice cloud amount, latent heating, and convective intensity indirectly through the mechanisms discussed above). In addition, high humidity at mid-levels has been shown to be critical for a cloud cluster to develop into a TC (Emanuel 1994; DeMaria et al. 2001). Thus the higher mid-level humidity in developer environments most certainly was a factor in the development of those clusters into TCs. Therefore, the humidity measurements prevent a definitive conclusion that aerosol loading surrounding developers helped cause their taller clouds, more prevalent ice clouds, greater latent heating, more intense convection, and their development into TCs since the high humidity surrounding developers can explain all of those things. To fully understand the relationship between aerosols and TC formation, the influence of aerosols must be separated from the influence of humidity.

To achieve this separation, the humidity effect was "removed": all of the analyses in this chapter were repeated using only cloud clusters with environments of roughly the same humidity. The RH at 500 hPa and 950 – 1000 km radii from the center of the clusters was used as a measure environmental humidity. The 500 hPa level was used because, as Fig. 2.6 shows, maximum developer minus nondeveloper differences for RH at outer radii are near 500 hPa. We

used the 950 – 1000 km radii zone to avoid contamination by water vapor outflow from the clusters. We assumed the RH at these radii was similar to the RH immediately outside the clusters (minus the humidity from outflow). The environmental RH for all of the developers and nondevelopers together ranged from 8 to 70%. To "remove" the influence of environmental humidity, only developers and nondevelopers with environmental RH between 37.5 and 46 % were analyzed. We refer to these cloud clusters as "moderate RH" developers and nondevelopers.

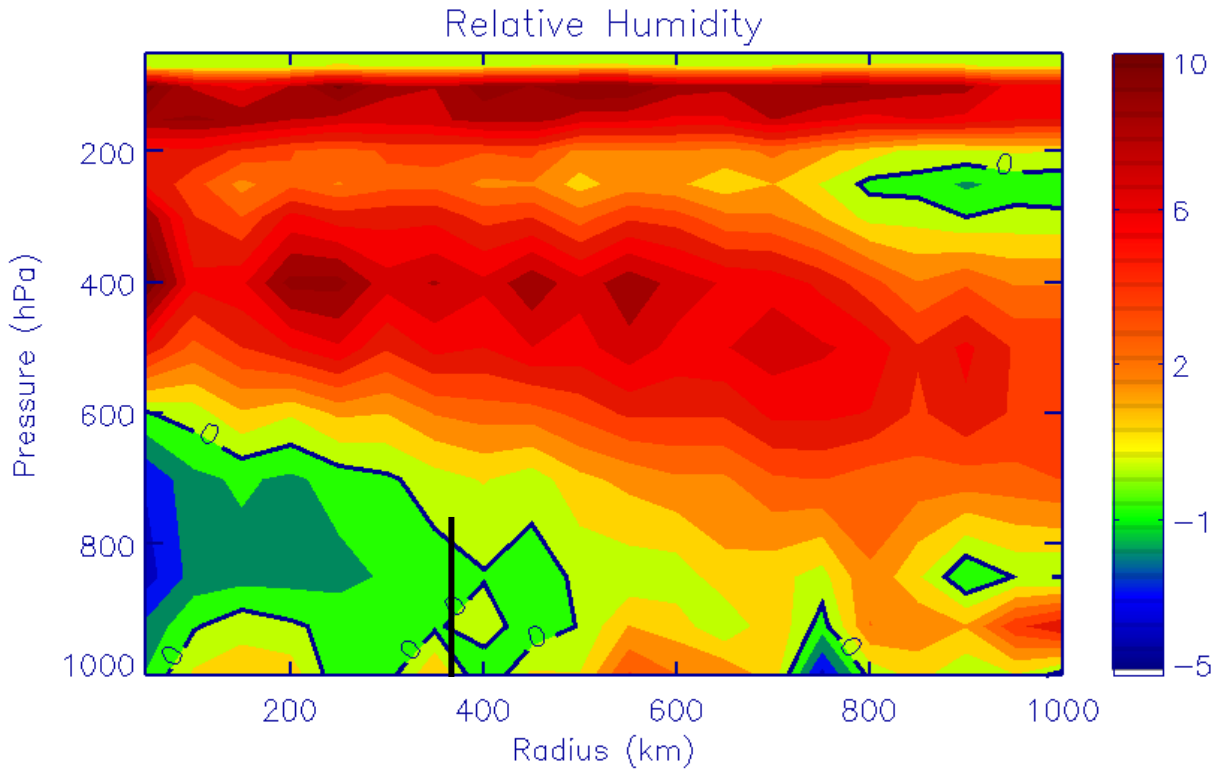


Figure 2.6: Azimuthal means of relative humidity in and near developers minus the same for nondevelopers as a function of height and radius from storm center.

Figure 2.7 shows mean environmental AOD for moderate RH developers minus that for moderate RH nondevelopers. Aside from more missing data, this plot generally looks similar to

the corresponding plot that was constructed using all developers and nondevelopers (Fig. 2.1). The difference between mean AOD near moderate RH developers and nondevelopers is larger than the difference for all of the developers and nondevelopers (compare Tables 2.2 and Table 2.1). Likewise, the moderate RH differences for all of the other parameters related to convective invigoration by aerosols are about the same or larger than those for all of the developers and nondevelopers (Tables 2.2 and 2.1). This suggests that the results related to more vigorous convection which were arrived at using all the cloud clusters (Figs. 2.3 through 2.5 and Table 2.1) were not necessarily due to higher humidity in developer environments, and further suggests that aerosols can indeed help cloud clusters develop into TCs by invigorating their convection. However, most of the differences in Table 2.2 are only significant at the 88% level or below. So no firm conclusions can be drawn from the moderate RH analysis. Furthermore, there are four environmental parameters in addition to mid-level humidity which also have been shown to be critical for cloud clusters to develop into TCs (Gray 1979; Emanuel 1994; DeMaria et al. 2001). Even if the positive correlation between aerosols and TC formation had been conclusively separated from the influence of humidity, it still could not be concluded that aerosols are a factor in TC development because some, or all, of these other four environmental factors may have been more favorable for development in developer environments. The influence of aerosols must be isolated from the influence of all five of the other environmental parameters before assessing whether or not aerosols are also a critical factor for TC formation. The evidence presented herein demonstrates that such research is warranted.

There is another issue related to humidity – the effect of humidity on AOD. As mentioned in Section 2.3.1, larger numbers of aerosols in the atmosphere result in larger values of AOD. But aerosol size and scattering coefficient also affect AOD. Larger aerosols and/or

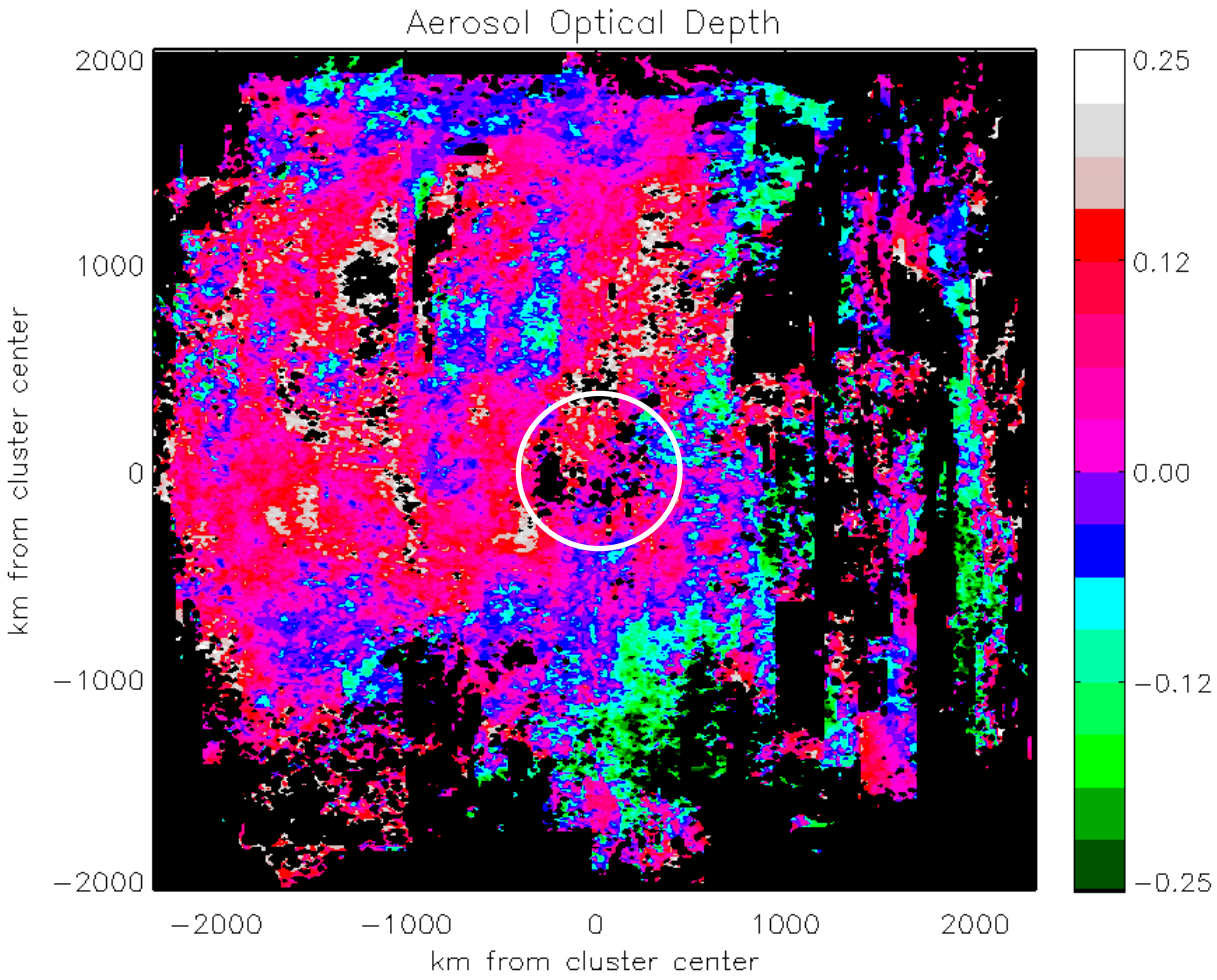


Figure 2.7: Composite mean AOD in and surrounding "moderate RH" developers minus the same for "moderate RH" nondevelopers. The white circle at the center represents a typical size for developers and nondevelopers. AOD is unitless.

aerosols with larger scattering coefficients result in larger values of AOD. When relative humidity is high, water vapor condenses on many aerosols, increasing their size and scattering coefficient – i.e., AOD is positively correlated with relative humidity. (Yoon and Kim 2006; Altaratz et al. 2013; Liu and Li 2014). One might suspect that the high RH in developer

Table 2.2: Parameters, for "moderate RH" developers and nondevelopers, related to invigoration of convection by aerosols. AOD was averaged over a box centered on storm center, 1200 km on each side. Cloud particle radius, cloud top pressure, and ice cloud percentage were averaged over a similar box, 400 km on each side. Temperature, a proxy for latent heating, was averaged from storm center to a radius of 250 km and between 500 and 250 hPa. Units for the means and standard deviations: microns for cloud particle radius, hPa for cloud top pressure, and K for the latent heating proxy. AOD is unitless. Sample size refers to the number of developers or nondevelopers. A positive percent difference means developer values are larger. Significance refers to the probability that the difference between means did not occur by chance, as determined by Student's t test. The (-20) next to the percent difference for cloud particle radius refers to the corresponding percent difference in cloud particle volume.

| | Mean | Standard Deviation | Sample size | Percent Difference Between Means | Significance (%) |
|---|---|---|---|---|---|
| AOD | | | | 52 | 99.8 |
| Developers | .278 | .118 | 14 | | |
| Nondevelopers | .183 | .067 | 29 | | |
| Cloud Particle Radius | | | | -6 (-20) | 87 |
| Developers | 26.0 | 2.07 | 14 | | |
| Nondevelopers | 27.6 | 3.35 | 28 | | |
| Cloud Top Pressure | | | | -8 | 88 |
| Developers | 220 | 32.2 | 14 | | |
| Nondevelopers | 239 | 37.4 | 29 | | |
| Ice Cloud Percentage | | | | 10 | 75 |
| Developers | 81.3 | 12.4 | 14 | | |
| Nondevelopers | 74.0 | 21.4 | 28 | | |
| Latent Heating Proxy | | | | 225 | 97 |
| Developers | 1.18 | 0.80 | 13 | | |
| Nondevelopers | 0.36 | 3.72 | 29 | | |

environments (Fig. 2.6) biased the AOD measurements – i.e., one might suspect the higher AOD measurements developers have compared to nondevelopers might not be due to larger numbers of aerosols, but instead may be due to the influence of high RH on aerosols.

However, at mid-range RH, such as that generally found near the cloud clusters of this study (not shown), substantial increases in AOD only occur when RH is increased by 20% or more (Yoon and Kim 2006), and the largest developer minus nondeveloper RH differences – either inside the clusters or in their environments – are less than 10% (Fig. 2.6). The largest RH differences are at midlevels. At 500 hPa, mean environmental RH (calculated using the same 1200 km box used to compute the mean environmental AOD in Table 2.1) for developers is only 5.37% higher than mean environmental RH for nondevelopers (developer RH is 52.6% and nondeveloper RH is 47.2%). Moreover, aerosol concentrations are usually highest at low levels (Seinfeld and Pandis 2006) and the differences between developer and nondeveloper RH at low levels are not nearly as large as those at midlevels (Fig. 2.6). At 925 hPa, mean environmental RH (calculated with the same 1200 km box) for developers is only 0.66% higher than mean environmental RH for nondevelopers (developer RH is 76.0% and nondeveloper RH is 75.3%). The moderate RH data in Fig. 2.7 and Table 2.2 demonstrate that the higher AOD in the environment of at least some of the developers is due to more aerosols and not higher humidity (the AOD difference in Table 2.2 is significant at the 99.8% level). As a more challenging test, AOD was averaged for subsets of the cloud clusters wherein nondevelopers had higher levels of environmental RH than developers. The same measurements used to define the moderate RH cloud clusters (RH at 500 hPa and 950 – 1000 km radius) were used as a measure of environmental RH for this analysis. AOD was averaged for all nondevelopers with environmental RH greater than 43.5% and for all developers with environmental RH less than 43.5% (the 43.5% value splits the populations for both types of cloud clusters roughly in half). Calculating means with these subsets still yields mean AOD for developers that is higher than mean AOD for nondevelopers – developer AOD is 0.247 and nondeveloper AOD is 0.208 (22

and 37 samples, respectively). In fact, these means are similar to those calculated using all of the developers and nondevelopers (Table 2.1). The subset results are inconclusive in that the difference between means is only significant at the 89% level, but when they are considered with all of the other information in this paragraph, it seems very unlikely that the AOD measurements originally discussed herein (the AOD for all developers and all nondevelopers) were impacted in a substantial way by the higher RH in developer environments.

Where did the high aerosol content surrounding developers come from? It is logical to suspect the dusty Saharan Air Layer (SAL). The SAL is an air mass that originates over the Sahara Desert and often migrates over the tropical Atlantic. The SAL is dry throughout the troposphere, especially at midlevels, and usually contains many aerosols, particularly mineral dust (Dunion and Velden 2004; Dunion 2011). The SAL often enhances convection along its western and southern borders (Chen 1985). Perhaps more developers had contact with the SAL than nondevelopers, and perhaps the SAL supplied the developers with abundant aerosols that invigorated convection. We investigated these possibilities by looking for evidence of the SAL near developers.

The SAL does not have a distinct temperature signature – the mean vertical temperature profile of the SAL is virtually identical to the climatological mean vertical temperature profile for the tropical North Atlantic (Dunion 2011). However, because of its aridity, the presence or absence of the SAL is reflected in moisture measurements, with midlevels (the driest levels of the SAL) impacted the most. Figure 2.8 shows the vertical structure of mean water vapor mixing ratio in and near developers, azimuthally averaged for different radii from storm center, minus the same for nondevelopers. Developer mixing ratios are larger throughout the troposphere, even hundreds of kilometers away from the clusters, suggesting the SAL was less prevalent in

developer environments compared to nondeveloper environments. Thus it appears that the higher aerosol content in developer environments (Fig. 2.1) did not come from the SAL; it appears the higher aerosol content near developers came from other sources.

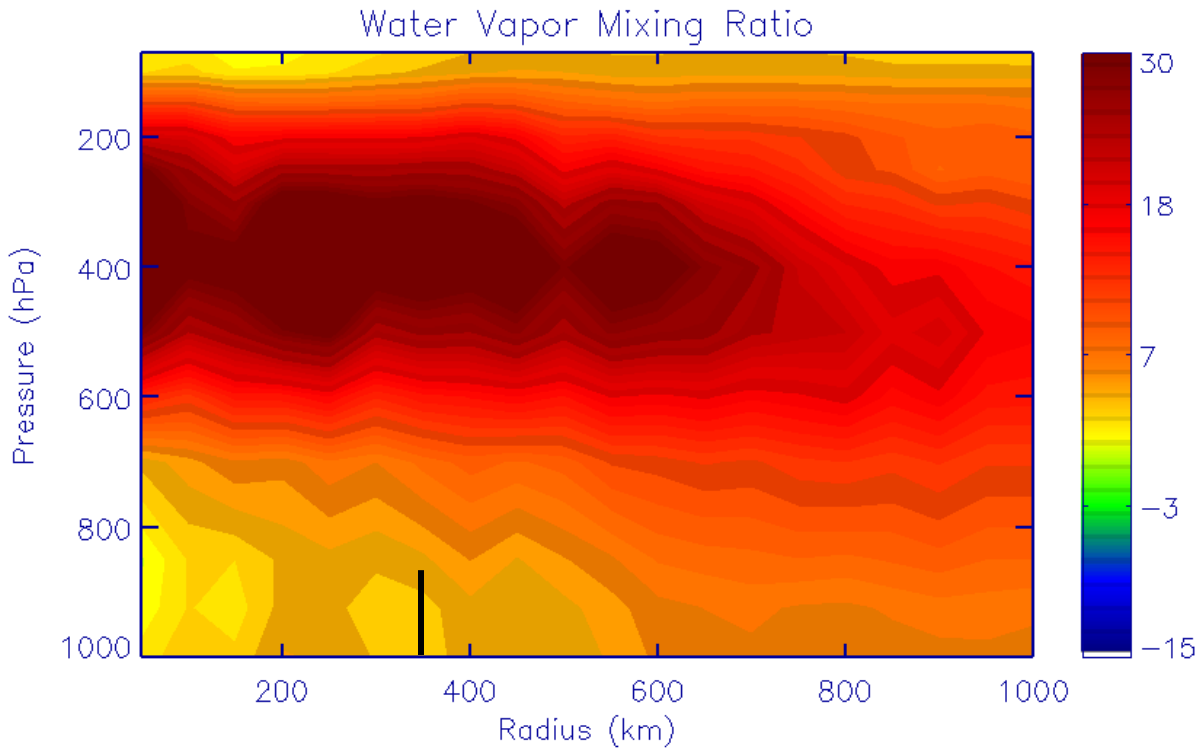


Figure 2.8: Azimuthal means of water vapor mixing ratio in and near developers minus the same for nondevelopers as a function of height and radius from storm center. Differences are plotted as percent differences: developer minus nondeveloper values divided by nondeveloper values.

## 2.5 Conclusions

We tested whether or not high aerosol concentrations in the environment of a tropical convective cloud cluster increase the likelihood that the cluster will develop into a TC by enhancing the convection within the cluster. We used AOD, as retrieved by the MODIS satellite instrument, as a measure of aerosol content. We examined the AOD surrounding all convective cloud clusters in the Atlantic that the NHC identified as having a good chance of developing into

a TC during 2005, 2006, 2007, and 2008. The AOD surrounding clusters that developed into TCs was significantly higher than that for clusters that did not develop into TCs – over 24% higher on average – suggesting that convective cloud clusters imbedded in regions of elevated aerosol levels have a substantially higher chance of developing into TCs compared to clusters imbedded in regions with lower aerosol concentrations. By itself, this is a noteworthy result.

Then, using other satellite data from MODIS and AIRS, we provided evidence that ingestion of high aerosol concentrations by developers led to a certain sequence of events – the well documented invigoration of convection by high aerosol content – that helped the developers make the transition into TCs. First in the sequence, high aerosol content leads to more numerous, and smaller, cloud droplets – we showed cloud particle sizes for developers are, on average, smaller than those for nondevelopers. Second, the smaller, lighter droplets are lofted to higher, colder altitudes – we showed cloud tops are typically higher in developers than in nondevelopers. Third, the colder temperatures cause the droplets to freeze – we illustrated the percentage of clouds that are ice clouds is higher for developers compared to nondevelopers. Fourth, when the droplets freeze, they release latent heat – we showed upper level temperatures (which were used as a proxy for latent heat release) in developers are higher than those in nondevelopers. Finally, the extra latent heat released by the freezing creates more buoyancy and thus stronger updrafts (i.e., stronger convection) – indirect evidence of stronger convection in developers was presented. Strong convection is essential for a cloud cluster to develop into a TC, so it follows that the high aerosol concentrations that the developers were exposed to invigorated their convection which helped them make the transition into TCs.

However, it could not be concluded that aerosols are definitely a factor in the developers' enhanced convection or in the developers' evolution into TCs because previous studies have

shown other environmental variables to be important for strong convection and TC formation, and some, or all, of these other variables may have been more favorable for convection and formation in developer environments. In fact, we showed that one of the variables, midlevel humidity, was more favorable for the developers. This alone could account for our results related to invigorated convection in developers and for the fact that the developers evolved into TCs, although a preliminary analysis aimed at separating the influences of aerosols and humidity indicated that ambient aerosol loading has a positive influence on convection/TC-formation that is independent of the influence from midlevel moisture. In the future, we plan to isolate the influence of aerosols from the influence of all of the other variables in order to determine whether or not aerosols are also a critical factor for TC formation. The evidence presented herein demonstrates that such research is warranted.

Because there is a well-known positive correlation between relative humidity and AOD, we performed several analyses in order to determine if the higher AOD developer environments had compared to nondeveloper environments was just an artifact of the higher humidity in developer environments. The analyses indicated it is very unlikely that humidity biased the AOD results in a substantial way.

Examination of tropospheric moisture fields near developers and nondevelopers unveiled no evidence that developers were usually closer to the SAL or spent more time near the SAL, and therefore the SAL is unlikely to have been a source of the extra aerosol loading developer environments had compared to nondeveloper environments.

The hurricane forecasters at NHC monitor cloud clusters where the environmental variables known to be important for TC development are favorable for TC development, but about 54% of the clusters inexplicably dissipate instead of developing into TCs (Jack Beven,

personal communication 2011; Dan Brown, personal communication 2017). Perhaps aerosol measurements in the vicinity of cloud clusters will give forecasters another tool that will help predict which clusters will develop into TCs and which will dissipate.

Although the final step of aerosol invigoration of convection – strong updrafts – cannot be measured directly with satellite instruments, Masunaga and Luo (2016) have developed a technique to infer updraft strength from satellite measurements. We plan to compare updrafts in developers and nondevelopers using Masunaga and Luo's technique in the near future. In addition, we will repeat the analyses of this study on tropical cloud clusters in other ocean basins.

# CHAPTER 3

## The Origin of Ozone in the Eyes of Mature Tropical Cyclones

### 3.1 Introduction

Several studies have found evidence of elevated ozone levels inside tropical cyclone eyes (Penn 1965; Rodgers et al. 1990; Zou and Wu 2005). The primary explanation behind the elevated ozone involves intrusion of ozone-rich stratospheric air downward into the upper and mid-troposphere of the eye. However, results from several other studies suggest there is little or no excess ozone within tropical cyclone (TC) eyes compared to the environmental basic state (Newell 1996; Carsey and Willoughby 2005; Joiner et al. 2006). Many of these studies conclude that a slightly lower tropopause (compared to the rest of the TC) over the eye accounts for any slight increases in ozone that might be detected.

Both types of results (evidence and no evidence of high ozone content) have come from studies using either aircraft or satellite data. Aircraft studies are limited in the sense they usually have very limited vertical and horizontal coverage – ozone measurements are usually only made at flight level and/or along the flight path. Lidar instruments mounted on planes cannot reliably detect ozone in clouds, which is important for comparing ozone in a TC's eye to ozone in the eyewall and elsewhere in the TC (Ravetta and Ancellet 2000). Satellite measurements also have limitations. It is rare that a satellite's orbit will take it directly over the eye of a TC; most TC eyes are far from nadir. This is problematic because the field-of-view (FOV) of a satellite instrument increases in size with distance from nadir and, as a result, FOVs far from nadir are often larger than a TC eye. Thus satellite measurements of eyes typically include information from clouds outside the eye. This is particularly an issue for measurements from older satellite instruments, as most older instruments had larger FOVs than the newer, more advanced instruments. Even at nadir, the FOV of older instruments may be larger than typical TC eyes. Furthermore, if an eye free of cirrus clouds is far enough from nadir, the clouds comprising the TC can obstruct the instrument's view of the bottom of the eye. In such cases, the instrument would only be able to observe the upper levels of the eye.

The purpose of this study is to provide clarification on whether large amounts of ozone are always, sometimes, or never present in the eyes of mature TCs by using analyses that avoid the limitations of aircraft measurements and the typical limitations of satellite measurements. We examine ozone in TC eyes using satellite data from instances when the relatively new Ozone Monitoring Instrument (OMI) passed directly over cirrus-free TC eyes. In these instances, the FOV can be small enough to fit entirely within the eye and the instrument has an unobstructed view of the eye all the way down to the bottom (the surface or the low stratus present in most TC

eyes). Thus ozone concentration in the eye can be assessed more accurately. The small FOV and overhead viewing angle also mean the location of anomalous ozone amounts with respect to the eye can be determined more accurately.

This study presents seven case studies: seven instances when OMI passed directly over the eye of a mature TC. In-depth analyses of multiple parameters are performed in order to determine the boundary of the eye for each storm (in order to determine whether ozone anomalies were located inside or outside the eye). When allowed by circumstances, ozone measurements for the day before or the day after OMI passed directly over the eye are examined so as to assess the progression of ozone patterns over time. The statistical significance of mean ozone amounts in and near the eye – compared to amounts throughout the rest of the TC and from the surrounding environment – is computed. In addition, the robustness of the results is tested by analyzing the measurements as a function of potential sources of bias.

The results lead us to pose a new theory for the source of elevated ozone in TC eyes and an explanation as to why elevated ozone is not always seen in eyes.

## 3.2 Data

### 3.2.1 *OMI Data*

The OMI instrument (Levelt et al. 2006) on board the polar-orbiting Aura satellite, which is part of the A-train, provided the measurements of ozone and all other atmospheric parameters used in this study (version 3 of all parameters were used). The OMI algorithm used to retrieve total ozone is similar to that used for the Total Ozone Mapping Spectrometer. OMI uses sunlight reflected from the Earth's surface or clouds to measure total ozone (the ozone between the surface of the Earth and the top of the atmosphere). Sunlight can be reflected to OMI by portions

of a cloud well below cloud top and by the earth's surface underneath a cloud. To account for this, the algorithm for processing OMI data calculates an effective cloud top pressure which is greater than the actual cloud top pressure (Joiner et al. 2006). The ozone below effective cloud top is then estimated from climatology using a technique outlined in Vasilkov et al. (2004). OMI passed over each TC once a day during daylight hours and the local time of day was always about 1:45 pm. At nadir, the OMI FOV is an oval with 13 and 24 km axes.

OMI data are organized into rows that are perpendicular to the direction of satellite motion. Each row is comprised of 60 pixels which are collected by 60 detectors. Some detectors have a bias which often leads to a "striping" effect (also called a "row anomaly") visible in many of the satellite images in this paper. For example, in the upper right panel of Fig. 3.1, the short stripes of high values south of the eye which are oriented in roughly the north-south direction are a result of a striping bias. The values in a given stripe correspond to the same detector. The stripes south of the eye in Fig. 3.1 all correspond to detector 31, which frequently has a striping bias. Striping biases are inconsistent in that they are not always present. Reflection of extra solar radiation, such as sun glint, can trigger striping biases for detectors capable of producing them (Thomas Kurosu, personal communication, 2013). Due to the geometry associated with sunlight reflecting off a TC eyewall, the TCs of this study most likely experienced sunglint in the eastern sector of their eyewall when OMI was directly over the eye [OMI's sun-synchronous orbit ensured the sun was to the west of the eyes and eyewalls are usually bowl-shaped (they usually slope away from TC center with height, often at an angle around 45º; Houze 2010)]. Since the FOV associated with detector 31 is right next to nadir, the eastern sector of the eyewall for the TCs of this study was often observed by detector 31. Thus OMI data for most of the TCs of this study contain a striping bias for the eastern eyewall. Note that Fig. 3.1 has a short stripe just to

the east of the eye. No data from detector 31 were included in the quantitative analyses of this study. It does not appear that biases from any other detectors affected the analyses.

### **3.2.2** *TC data*

Various government agencies record TC center locations at least four times per day. Latitude and longitude for all center locations for all TCs occurring around the globe since the launch of OMI were obtained from the International Best Track Archive for Climate Stewardship (IBTrACS) data set (Knapp et al. 2010). To be included in this study, a TC must have had an OMI overpass within 18 km of one of the center locations. Unless noted otherwise, all TCs analyzed had well-developed eyes free of upper level clouds.

Table 3.1 lists the TCs analyzed in this study. Damrey, Ioke, and Jova were all at peak intensity when OMI passed over the eye (Ioke weakened and re-intensified three times; OMI passed over the storm during its fourth peak intensity, which is shown in Table 3.1). Khanun, Saomai, and Xangsane were all within nine hours and 11 hPa of peak intensity at the time OMI passed over the eye. OMI passed over Dora's eye about 1.5 days before peak intensity, at which point the central pressure was 35 hPa greater than that at peak intensity.

Table 3.1: Tropical Cyclones analyzed in this study. All data pertain to the date listed for each storm.

| Name | Date | Location | Latitude | Longitude | Central Pressure (hPa) |
|---|---|---|---|---|---|
| Damrey | Sep. 25, 2005 | NW Pacific | 19.1 | 112.4 | 955 |
| Dora | Feb. 1, 2007 | SW Indian Ocean | -15.3 | 67.5 | 960 |
| Ioke | Aug. 31, 2006 | NW Pacific | 18.9 | 168.0 | 920 |
| Jova | Sep. 19, 2005 | NE Pacific | 15.9 | -143.2 | 951 |
| Khanun | Sep. 10, 2005 | NW Pacific | 24.0 | 125.5 | 950 |
| Saomai | Aug. 10, 2006 | NW Pacific | 26.9 | 121.3 | 935 |
| Xangsane | Sep. 27, 2006 | NW Pacific | 12.9 | 124.7 | 927 |

### 3.3 Analysis of TC ozone

#### **3.3.1** *Saomai, Jova, Khanun, and Xangsane*

Figure 3.1 shows total ozone for Typhoon Saomai on 10 August, 2006 (upper right and lower left panels) along with the storm's reflectivity, which is similar to a visual image (left panel). About 85% of the tropical atmosphere's ozone is in the stratosphere (Seinfeld and Pandis 2006), but it is highly unlikely that the mesoscale ozone variations in Saomai are due to ozone variability in the stratosphere – ozone variations in the stratosphere tend to occur over hundreds or thousands of kilometers. The ozone patterns match very well with the cloud patterns shown in the left panel, indicating most of the ozone variability is associated with processes taking place in Saomai. The OMI instrument detects ozone well within clouds – for deep convection, OMI typically measures ozone 300-400 hPa below cloud top with little attenuation (Vasilkov et al. 2008). Thus, most of Saomai's ozone variability is most likely a reflection of ozone concentrations embedded in convective and cirrus clouds.

In order to analyze just the tropospheric/very low stratospheric portion (hereafter, "tropospheric portion") of the total ozone measurements, we removed an estimate of the stratospheric portion. We assumed stratospheric ozone concentrations were very uniform over Saomai and the nearby environment, and estimated the stratospheric portion in the region as 85% of the mean total ozone outside Saomai but within 2º latitude of storm center and within the lateral ken of the OMI instrument (1300 km east or west of storm center). Only observations from locations that were over the ocean and had no clouds or low clouds were included in the mean. The stratospheric estimate was 230.4 Dobson Units (DU) and was subtracted from all total ozone data for Saomai and the nearby environment before performing any quantitative analyses. Tropospheric ozone for the other TCs was calculated the same way.

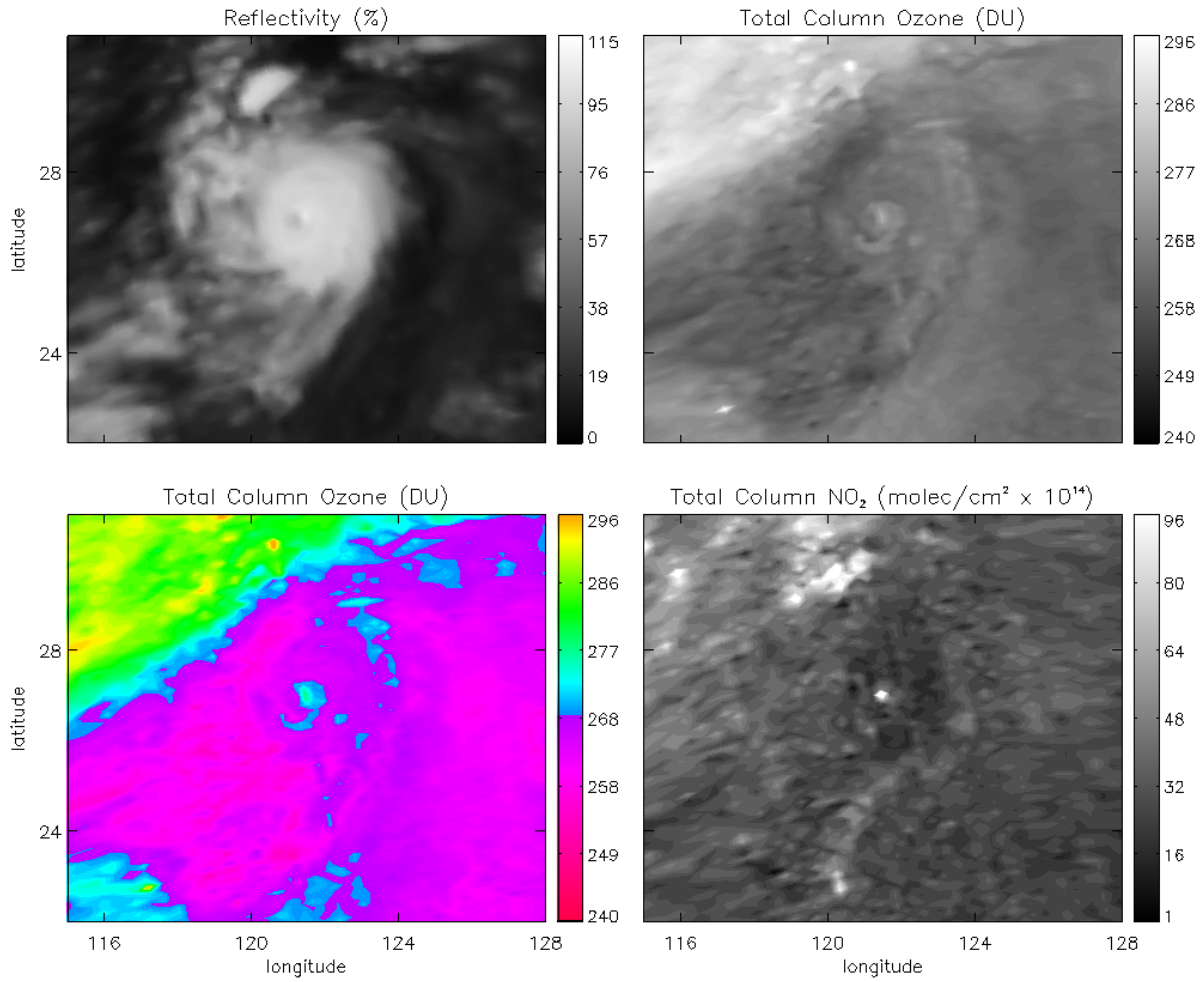


Figure 3.1: Typhoon Saomai, 5:21 GMT on 10 August, 2006; (upper left) reflectivity; (upper right) total ozone; (lower left) total ozone with color scheme added; (lower right) total $NO_2$. All data measured by the OMI instrument.

Ozone levels in a comma-shaped area within 100 km of the center of the storm are high compared to levels elsewhere within the storm (Fig. 3.1, upper right, lower left). The elevated ozone appears to be in the eyewall, part of a rainband, and possibly the eye. Determination of whether or not the elevated ozone of the comma-shaped area (hereafter, the "comma") includes the eye is important for the purposes of this study. This determination requires the exact location of the eye. The eye location is determined by analyzing navigation, effective cloud-top pressure,

and reflectivity. The discussion of these three factors that follows refers to Fig. 3.2 which shows effective cloud-top pressure and reflectivity in and near Saomai's eye. The box within each panel of Fig. 3.2 represents the edge of the eye.

- *Navigation*: According to OMI navigation and Saomai's best track, the value of 726 hPa within the box (top panel) corresponds to the OMI FOV closest to the center of Saomai (the FOV center is 5 km away from storm center).
- *Effective cloud-top pressure:* The effective cloud top pressures within the box are much larger than those outside the box (top panel). The large pressures, both above 700 hPa, indicate the corresponding OMI FOVs contained low stratus clouds, which are present in most TC eyes. One might expect pressures greater than 800 or even 900 hPa for such clouds, however it is likely that the FOVs also included a little of the deep convective clouds comprising the eyewall. The values outside the box's contour range from 370 to 544 hPa. These values represent deep clouds of the eyewall or possibly high thick cirrus of the TC cloud shield.
- *Reflectivity*: OMI reflectivity values indicate the percent of sunlight at 360 nm reflected by clouds and the earth's surface back to OMI. Reflectivity for OMI is defined in such a way that it can be as large as 115%. Near TCs, large values primarily result from thick clouds, but can also result from rain, snow and/or graupel (Joanna Joiner, personal communication, 2013). Since deep convective clouds are thicker and produce more precipitation than stratus or cirrus, they reflect more sunlight. The middle panel of Fig. 3.2 shows the reflectivity near Saomai's eye and supports the delineation of the eye as determined from effective cloud top pressure (the box). The two values inside the box are 82 and 84% (the two smallest values in the figure), while most of the values outside

the box are well over 90% (the even larger values with lines drawn through them were obtained by detector 31 and correspond to the highly reflective eastern sector of the eyewall, and thus are most likely spuriously large – see the discussion of the striping effect in Section 3.2.1). The large values surrounding the box indicate the presence of deep convection, while the smaller values inside the box reflect the presence of the low stratus clouds in Saomai's eye and most likely would be smaller but the FOVs for the two values most likely included some of the highly reflective eyewall.

With the boundaries of the eye established, determination of whether or not the elevated ozone of the comma includes the eye is now possible. The bottom panel of Fig. 3.2 shows the tropospheric ozone near Saomai's eye. The values inside the eye (34 and 36 DU) are noticeably lower than values in the comma, which range from the upper 30's to lower 40's (the comma surrounds the eye except to the northwest). The mean ozone in the eye (35.1 DU) is 13% less than the mean for the comma (39.7 DU; Table 3.2). The difference is significant at the 99% level, as determined by the Mann Whitney U test. The ozone in the eye is slightly elevated compared to the ozone found throughout most of Saomai – the mean for the eye is 5% higher than the mean for the cloud shield outside of the comma – while the mean for the comma is substantially higher than the mean for the cloud shield (19% higher; Table 3.3). The eyewall/cloud shield difference is statistically significant at the 99.9% level. Thus, Saomai's large positive ozone anomalies are in the eyewall, not the eye as one would expect given the previous studies cited in Section 3.1.

The boundary of the eye was determined for the other TCs of this study using the same methods illustrated in Fig. 3.2. Table 3.3 shows ozone concentrations in Hurricane Jova's eyewall were slightly elevated (6% higher than the rest of the cloud shield), although in two

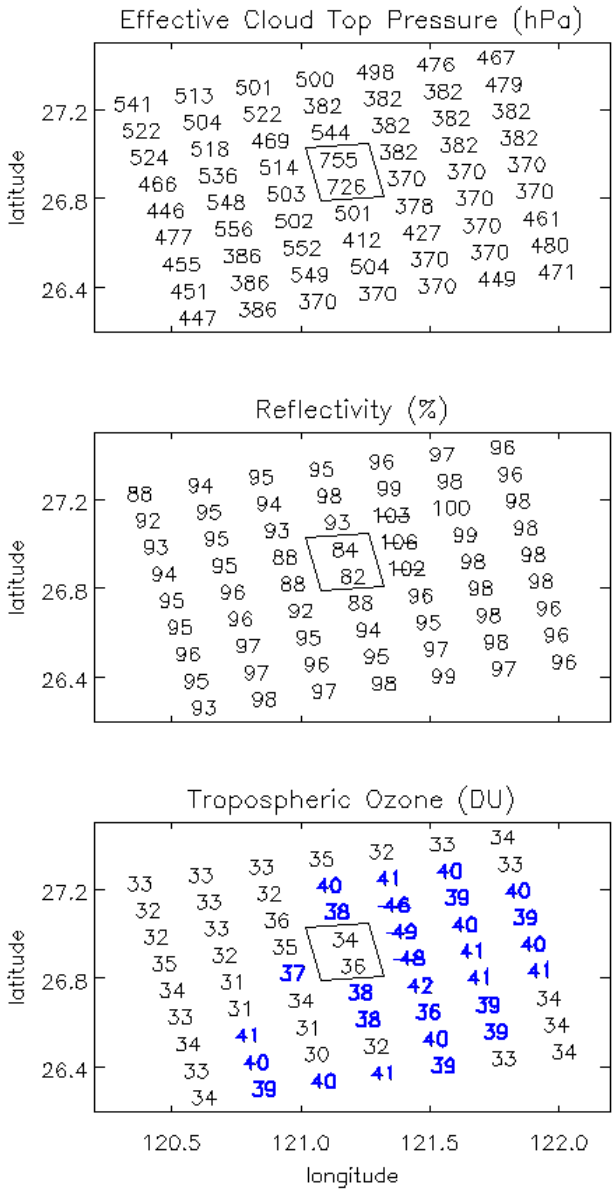


Figure 3.2: (top) effective cloud top pressure; (middle) reflectivity; (bottom) tropospheric ozone in and near the eye of Typhoon Saomai. Measured by the OMI instrument on the same date and time as in Fig. 3.1. The box represents the boundary of the eye. Blue indicates values from the "comma" (locations in and near the eyewall with elevated ozone). A line through a number indicates the value was most likely influenced by the "striping" bias described in the text.

Table 3.2: Mean tropospheric ozone inside the eye (first column); mean tropospheric ozone in and near the eyewall (second column); difference between first and second columns (third column); probability, as determined from the Mann Whitney U test, that differences in third column occurred by chance (fourth column). Sample size refers to the number of OMI measurements in each area (no measurements from detector 31 are included). The data in this table correspond to Figs. 3.1, 3.3, 3.4, and 3.6.

| TC Name | Eye (DU) | In/near Eyewall (DU) | Difference (DU) | Sample Size | | Probability |
|---|---|---|---|---|---|---|
| | | | | Eye | Eyewall | |
| Saomai | 35.1 | 39.7 | -4.6 | 2 | 23 | .0033 |
| Jova | 29.4 | 36.5 | -7.1 | 2 | 79 | .0003 |
| Ioke | 37.3 | 39.4 | -2.1 | 6 | 14 | .0007 |
| Damrey | 40.6 | 35.1 | 5.5 | 10 | 23 | .0001 |

portions of the eyewall, positive ozone anomalies were more substantial (Fig. 3.3, right panel). Ozone levels in the eye were much lower than those in the eyewall (Table 3.2). In fact, they were low in an absolute sense – i.e., they were low when compared to ozone levels in the environment surrounding Jova. Table 3.4 compares the mean amount of ozone in the eye to the mean amount in the environment. Only data from locations in Fig. 3.3 with effective cloud tops between 862 and 884 hPa (the two effective cloud top pressures inside Jova's eye) were included in the average for ozone outside of Jova (locations also had to be over the ocean and within 2 degrees latitude of Jova's center). The amount of ozone in Jova's eye is exceedingly small compared to the environment (the environmental mean is 36% higher).

Ozone amounts in Typhoon Khanun's eyewall were 13% larger than those in the rest of the cloud shield (Table 3.3). Khanun had very small amounts in the eye, but data for Khanun's eye are not included in this study because only one OMI FOV fit inside Khanun's small eye and

Table 3.3: Mean tropospheric ozone in and near the eyewall (first column); mean tropospheric ozone for the rest of the cloud shield (second column); inner and outer boundaries of the cloud shield (not including the eyewall), expressed as radii from storm center (third column). The number of OMI measurements in each area (fourth and fifth columns; no measurements from detector 31 are included). The probability, as determined by the Mann Whitney U test, that the difference between the values in the first and second columns occurred by chance (last column). The data in this table correspond to Figs. 3.1, 3.3, and 3.4 (data for Khanun are not shown in a figure).

| TC name | Eyewall (DU) | Cloud Shield (DU) | Cloud Shield Boundaries (km) | Sample Size | | Probability |
|---|---|---|---|---|---|---|
| | | | | Eyewall | Cloud Shield | |
| Saomai | 39.7 | 33.5 | 100-255 | 23 | 494 | <.0001 |
| Jova | 36.5 | 34.3 | 100-220 | 79 | 349 | <.0001 |
| Ioke | 39.4 | 30.8 | 50-250 | 14 | 533 | <.0001 |
| Khanun | 33.3 | 29.6 | 55-118 | 21 | 98 | <.0001 |

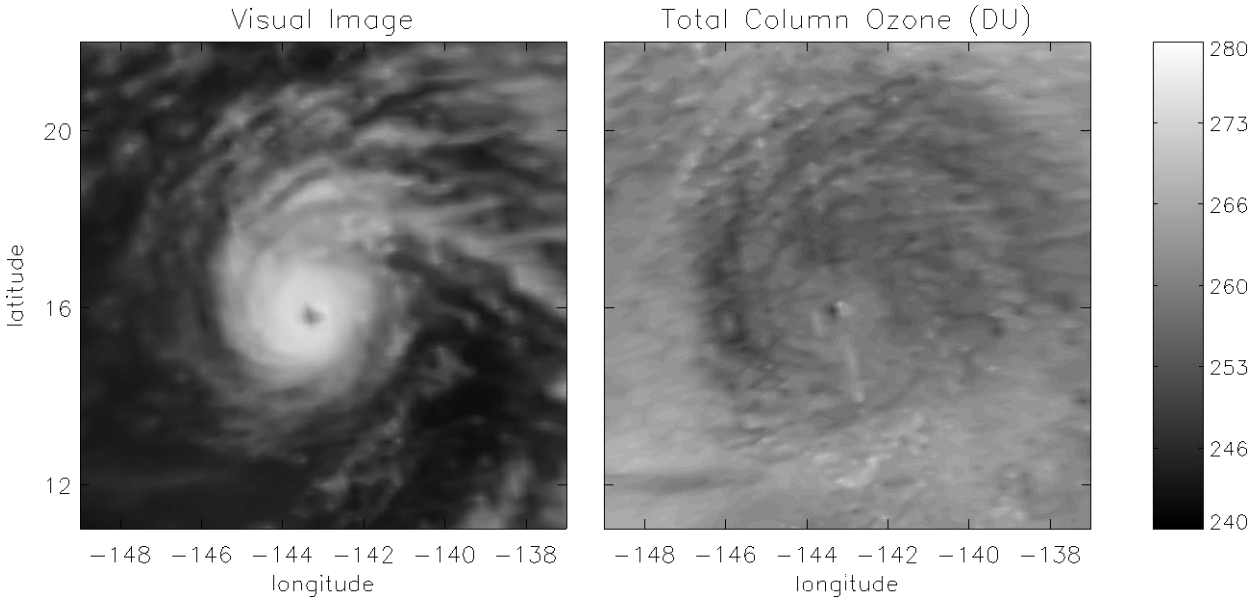


Figure 3.3: Hurricane Jova, 23:03 GMT on 19 September, 2005; (left panel) reflectivity; (right panel) total ozone. Both parameters were measured by the OMI instrument.

Table 3.4: Mean tropospheric ozone in the eye (first column) and in the nearby environment outside the TC (second column). The number of OMI measurements in each area (third and fourth columns; no measurements from detector 31 are included). Ozone values outside the TCs only pertain to locations that are over the ocean, are within 1300 km east or west of TC center, are within 2º latitude north or south of TC center, and have effective cloud top pressures within the range of those inside the eye). The data in this table correspond to Figs. 3.1, 3.3, 3.4, and 3.6 (data for Xangsane are not shown in a figure).

| | Tropospheric Ozone (DU) | | Sample Size | |
|---|---|---|---|---|
| | In eye | Outside of TC | In eye | Outside of TC |
| Saomai | 35.1 | 34.8 | 2 | 7 |
| Jova | 29.4 | 39.9 | 2 | 28 |
| Ioke | 37.3 | 38.7 | 6 | 19 |
| Xangsane | 30.3 | 42.1 | 3 | 23 |
| Damrey | 40.6 | 38.5 | 9 | 15 |

that FOV was measured by detector 31 (see Section 3.2.1). Typhoon Xangsane's eyewall had large amounts of ozone, but the data for the FOVs with large amounts showed signs of corruption (the retrievals of effective cloud top pressure were of poor quality) which puts the authenticity of the large values into question. Therefore only data from Xangsane's eye is included in this study. Like Jova, Typhoon Xangsane had an exceedingly small amount of ozone in the eye. The mean amount of ozone in Xangsane's eye was 11.8 DU smaller than that in the surrounding environment – the largest difference in Table 3.4.

### **3.3.2** *Ioke and Damrey*

Elevated ozone was also present in the eyewall of Typhoon Ioke (Fig. 3.4, upper right and lower left panels). Mean ozone in the eyewall was 28% larger than mean ozone in the rest of the cloud shield (Table 3.3). Figure 3.4, especially the colorized image in the lower left panel, indicates that the eye did not contain especially large amounts of ozone. However, the eye was larger than it appears in Fig. 3.4. Figure 3.5 shows OMI made six measurements in Ioke's eye

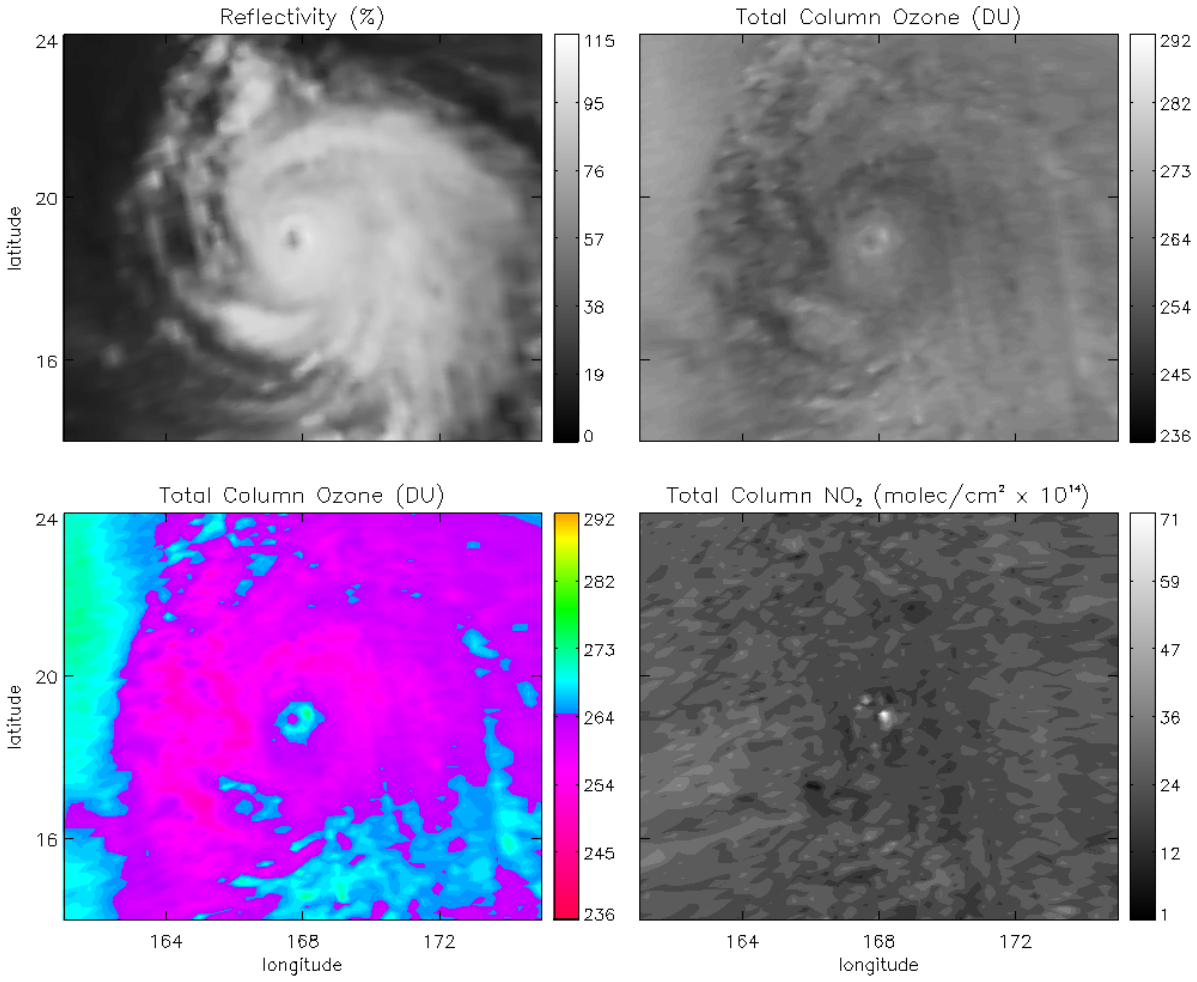


Figure 3.4: As in Fig. 3.1, but for Typhoon Ioke, 2:20 GMT on 31 August, 2006.

(i.e., there were six OMI FOVs in the eye). Two of the measurements are low (the average for the two is 16% lower than the eyewall average), but the other four measurements are high – they are comparable to those in the eyewall. The four high values appear to be part of the eyewall in Fig. 3.4 (lower left), while the two low values correspond to the magenta colored portion of the

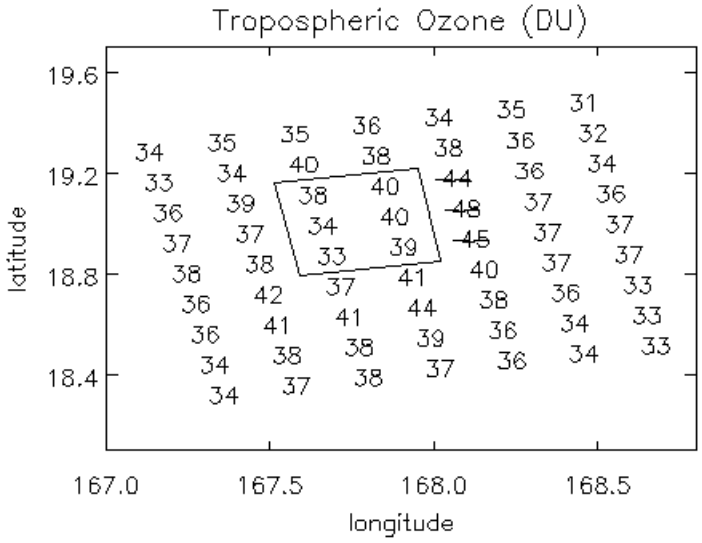


Figure 3.5: Tropospheric ozone in and near the eye of Typhoon Ioke. Measured by the OMI instrument on the same date and time as in Fig. 3.4. The box represents the boundary of the eye, which was determined using the same methods illustrated in Fig. 3.2. A line through a number indicates the value was most likely influenced by the "striping" bias described in the text.

eye. So in addition to the eyewall containing large amounts of ozone, parts of Ioke's eye also contain large amounts.

Typhoon Damrey was even more dissimilar from Saomai, Jova, Khanun, and Xangsane. Figure 3.6 (middle panel) shows Damrey did not have any ozone anomalies of note in the eyewall, and the almost the entire eye contained elevated ozone. Figure 3.7 confirms the elevated ozone was located in the eye. Values in the eye were predominantly equal to or greater than 40 DU, while those in the eyewall and elsewhere range from 33 to 38 DU (except for the values

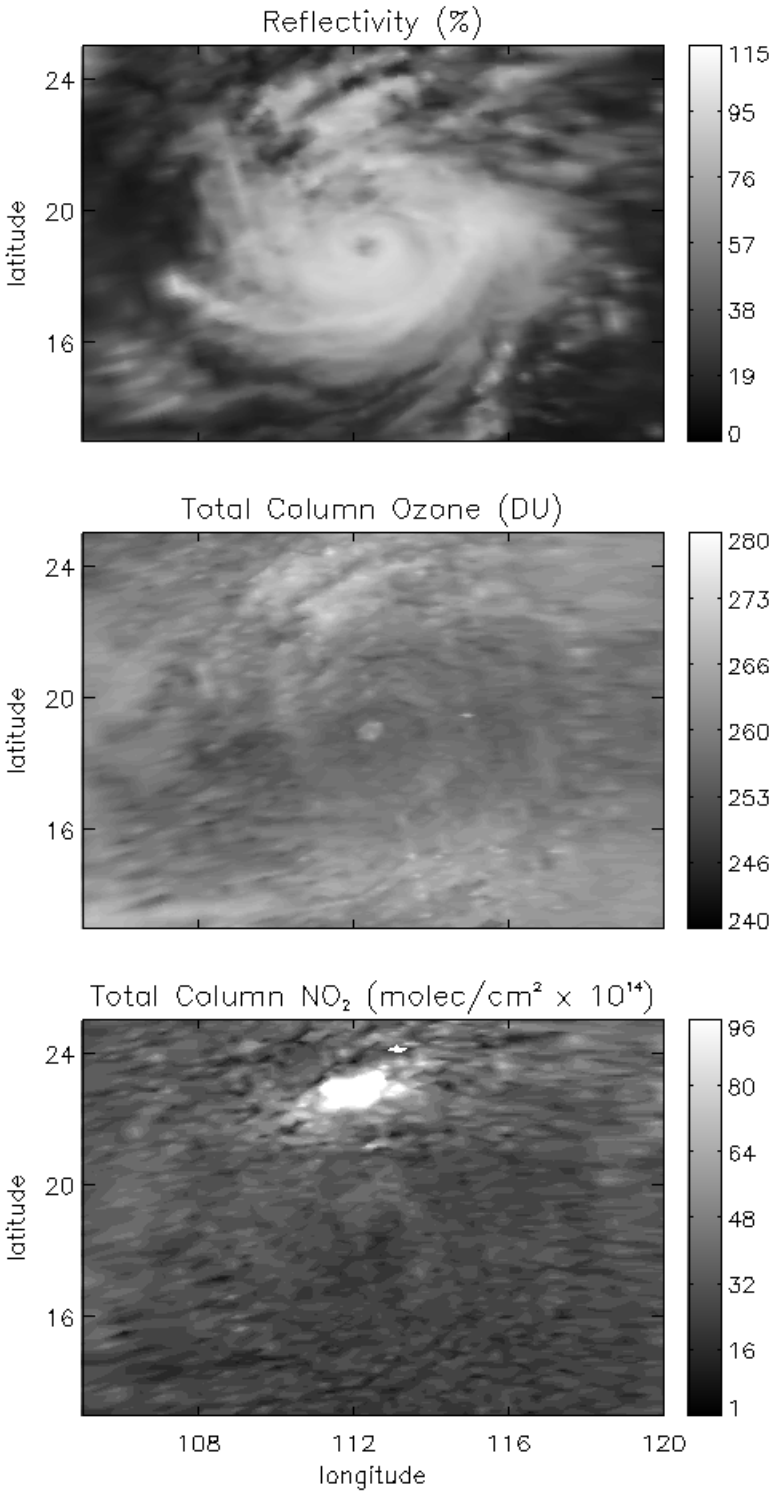


Figure 3.6: Typhoon Damrey, 5:58 GMT on 25 September, 2005; (top) reflectivity; (middle) total ozone; (bottom) total $NO_2$. All data measured by the OMI instrument.

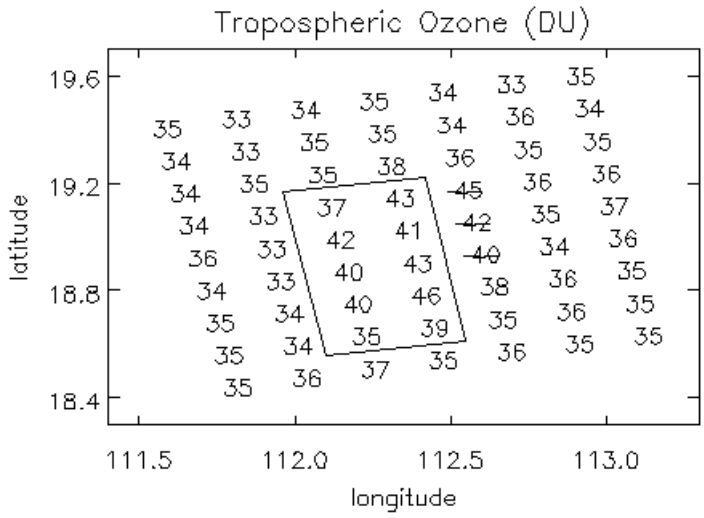


Figure 3.7: as in Fig. 3.5 but for Typhoon Damrey. Measured by the OMI instrument on the same date and time as in Fig. 3.6.

above 40 DU in the northeast quadrant of the eyewall, but those appear to be due to striping – they correspond to detector 31 and the eastern sector of the eyewall, see Section 3.2.1). The average amount of ozone inside the eye is 40.6 DU while the average in and within 30 km of the eyewall is only 35.1 DU (Table 3.2). The difference is 5.5 DU which means the amount of ozone in the eye is 16% larger than in/near the eyewall. In addition, the average for the eye is 2.1 DU larger than the average for the nearby environment outside of Damrey (Table 3.4).

### **3.3.3** *Analysis summary*

Elevated ozone levels were present in the eyewalls of Saomai and Jova. Both storms had lower ozone levels in the eye. Khanun had high ozone levels in the eyewall, but corrupted data in the eye prevents any conclusions about ozone in the eye. Xangsane had very low ozone levels in the eye, but corrupted data in the eyewall prevents any conclusions about ozone in the eyewall.

Ioke had a high amount of ozone in the eyewall and part of the eye had a low amount, but a large portion of the eye had a high amount. Damrey had no ozone anomalies of note in the eyewall, but almost the entire eye was filled with large amount of ozone.

## 3.4 Discussion

### 3.4.1 *Low Ozone Levels in the Eye*

The very low ozone levels in the eye of Jova and the eye of Xangsane (Tables 3.2 and 3.4) were most likely due to the "doming" effect described by Zou and Wu (2005; also see Fu et al. 2013). Updrafts and moist adiabatic cooling associated with convection elevate the tropopause over a TC. Elevation of the tropopause decreases with increasing radius from storm center, resulting in a dome-shaped tropopause over a TC with the highest tropopause height located over the eye. Since there is much less ozone in the troposphere than in the stratosphere, the increased vertical extent of the troposphere results in less total ozone for a TC compared to the surrounding environment. The smallest amount of total ozone is near the eye, at least when azimuthal means are considered (Fig. 3.8; a small ozone maximum near the eye observed in the raw data by Zou and Wu was rendered invisible by a smoothing technique they applied to the data). Inspection of the OMI imagery for the TCs of this study generally supports the results from Zou and Wu: low total ozone for most of the area occupied by TCs compared to the surrounding environment. An especially clear example is Jova (Fig. 3.9; this is the same as Fig. 3.3 but with more of the surrounding environment included). Thus, the most likely explanation for the low amount of ozone in Jova's and Xangsane's eye appears to be the doming effect.

### **3.4.2** *High ozone levels in the eyewall*

Elevated ozone was located in the eyewalls of Saomai, Jova, Khanun, and Ioke. High ozone levels were also often present in the cloud shield very close to the eyewall, and in Saomai's case, part of a rainband spiraling into the eyewall. As discussed in the Introduction, a low tropopause or subsidence of stratospheric air into the troposphere have been suggested to

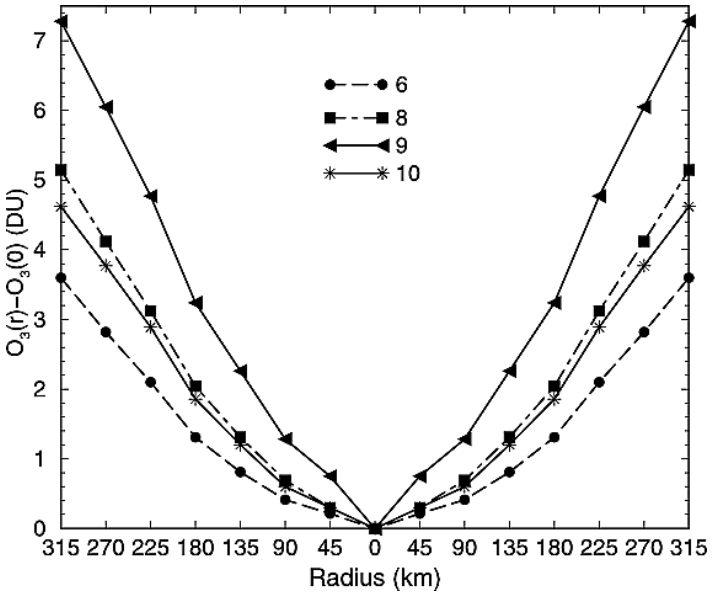


Figure 3.8: Radial profiles of Total Ozone Mapping Spectrometer (TOMS) $O_3$ for Hurricane Erin on 6, 8, 9, and 10 September 2001. The y-axis represents mean ozone at a given radius minus mean ozone over the eye. These radial total ozone profiles are obtained from smoothed gridded data with 45 km horizontal resolution. Reprinted from Zou and Wu (2005).

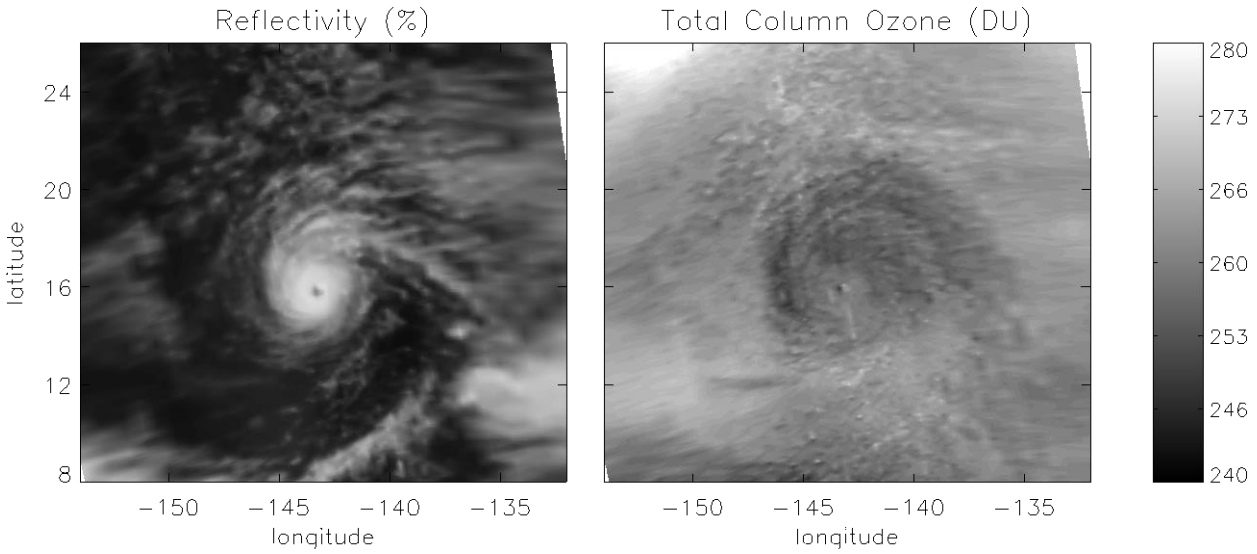


Figure 3.9: Same as Fig. 3.3, but more of the environment surrounding Hurricane Jova is shown.

cause high ozone levels in TC eyes, but the eyewall, cloud shield, and rainbands of a TC are primarily occupied by deep convection and/or thick cirrus, not by a low tropopause or subsidence. Analysis of infrared images from geostationary satellites and cloud-top pressure images from OMI confirm this is the case for the TCs of this study. So what could account for the high ozone values?

Lightning may provide the answer. Orville (1967) documented evidence that lightning catalyzes the formation of a substantial amount of ozone. More recently, Minschwaner et al. (2008) showed lighting can directly produce a 50% increase above mean background ozone in its vicinity. While TCs usually do not produce large amounts of lightning, occasionally they do (Abarca et al. 2011). Thus the deep convection in Saomai's, Jova's, Khanun's and Ioke's eyewall may have produced enough lightning to cause the high levels of ozone measured by OMI.

Lightning also produces ozone indirectly by catalyzing the formation of nitric oxide (NO), which quickly reacts to form nitrogen dioxide ($NO_2$; Huntrieser et al. 1998). Given enough

sunlight and enough volatile organic compounds (VOCs) in the presence of the $NO_2$, cyclic production of ozone will ensue. The supply of VOCs outgassed from the ocean by the high wind speeds and low atmospheric pressure of a TC may be sufficient to facilitate the production of ozone in a TC (Carsey and Willoughby 2005). The convection in a TC eyewall could transport the VOCs and $NO_2$ to the upper levels (Pickering et al. 1992; Thompson et al. 1997; Huntrieser et al. 1998) where ample sunlight is available for ozone production (DeCaria et al. 2005). However, previous studies have shown production of ozone from a convective cloud's lightning-generated $NO_2$ usually takes place in the cloud's outflow, not in the cloud itself, and substantial ozone amounts often do not accrue until hours after the cloud has dissipated (Pickering et al. 1996; Ott et al. 2007; Apel et al. 2015). Based on these studies, one would expect to see positive ozone anomalies in the eyewall's cirrus outflow – at a distance from the eyewall – not in the eyewall itself. But most of these studies focused on midlatitude thunderstorms (Kenneth Pickering, personal communication, 2017). Higher actinic flux allows for more rapid ozone production (Seinfeld and Pandis 2006) – perhaps the higher actinic flux in the tropics leads to the production of substantial amounts of ozone within the lifetime of the convective clouds of the eyewall. Or perhaps some of the eyewall $NO_2$ and VOCs can get caught in downdrafts and other turbulence in and near the eyewall, staying local long enough to produce ozone in the eyewall. Despite these possibilities, overall it seems more likely that the elevated ozone observed in the eyewalls is a result of direct production, not indirect production through $NO_2$, from lightning. OMI observations of $NO_2$ are discussed below.

Verification that lightning took place in the eyewalls would provide evidence for the hypothesis that lightning produced the excess eyewall ozone. Unfortunately, detailed lightning measurements are not available for the TCs of this study. The best measurements available for

these storms come from the World Wide Lightning Location Network (WWLLN) but, during the years the TCs of this study existed (2005-2007), the detection efficiency of the WWLLN was only about 5% (i.e., only about 5% of lightning strikes around the globe were detected; Abarca et al. 2010; Robert Holzworth, personal communication, 2013). Nevertheless, WWLLN data can be used to get a rough indication of lightning activity in the TCs we analyzed. Figure 3.10 shows the lightning strikes detected in Ioke during the two hour period before the OMI measurements of elevated ozone in the eyewall. The cluster of strikes near TC center indicates there was lightning activity in the eyewall. In general, the lightning measurements for the other TCs with elevated eyewall ozone are similar (not shown).

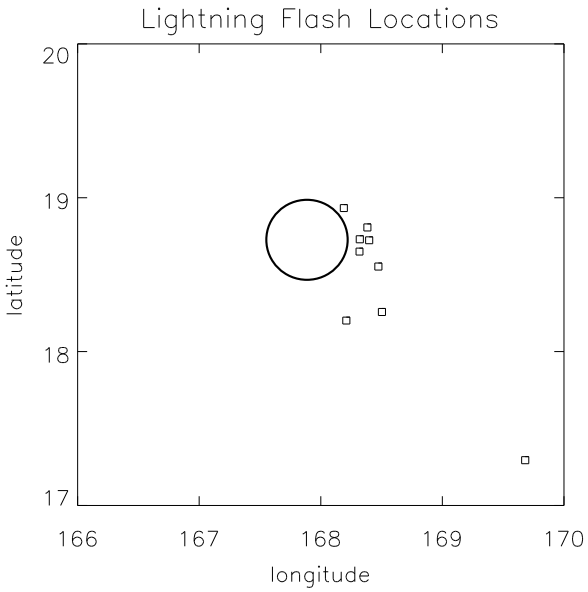


Figure 3.10: Lightning strikes, as detected by the WWLLN, in and near the eyewall of Typhoon Ioke during the two hours prior to the measurement of the ozone displayed in Fig. 3.4. Each square represents a strike. The circle represents the boundary of the eye.

Measurements of $NO_2$ provide indirect evidence of eyewall lightning. As discussed above, lightning catalyzes the formation of $NO/NO_2$. If lightning is behind the high ozone measurements in the eyewalls, one would expect to see high levels of NO and $NO_2$ in the same locations. OMI cannot measure NO, but it can measure $NO_2$. The lower right panel of Figure 3.4 shows total column $NO_2$ for Ioke at the same time the ozone in Fig. 3.4 was observed (upper right and lower left panels). High values of $NO_2$ are present in the eyewall, indicating lightning took place there. A strong, positive $NO_2$ anomaly is present in Saomai's eyewall, but does not cover as much area as the high ozone levels, which span most of the eyewall (compare the upper right and lower right panels in Fig. 3.1). In general, the high ozone anomalies in the eyewalls of the TCs of this paper cover more area than the high $NO_2$ anomalies. This is unexpected since most studies have found that lightning produces more $NO_2$ than ozone. However, there is much uncertainty about the amount of ozone and $NO_2$ produced by lightning. Schumann and Huntrieser (2007) estimate that a typical lightning flash produces $1.5 \times 10^{26}$ molecules of NO, while Minschwaner et al. (2008) show that lightning can produce as much as an order of magnitude more ozone ($1.6 \times 10^{27}$ molecules). Therefore, the greater areal coverage of ozone compared to $NO_2$ may be because the lightning in the eyewalls of the storms of this study simply produced more ozone than $NO_2$. If so, as ozone and $NO_2$ spread out away from a lightning bolt location, the $NO_2$ would have become diffuse to the point where the amount was no longer visibly elevated before the ozone would have, resulting in elevated ozone levels covering a larger areal extent (as is observed). Alternatively, the cyclic production of ozone by $NO_2$ noted above may explain why high ozone anomalies are more prevalent than high $NO_2$ anomalies. With cyclic production, one $NO_2$ molecule leads to the production of many ozone molecules. [It should be noted that the depth below cloud top to which the OMI instrument can detect $NO_2$ and

ozone is almost the same (Nickolay Krotkov, personal communication, 2017)]. Regardless of the area coverage, the high $NO_2$ anomalies in the eyewalls are strong indicators that lightning took place there.

If the observed elevated ozone was not a result of subsidence of stratospheric air into the eye or a low tropopause over the eye, but instead was a result of lightning in the eyewall and/or rainbands, then elevated ozone should be found in any eyewall or rainband that produces substantial lightning, even if the TC has a cirrus-covered eye or no eye at all. Jova, two days after the data in Fig. 3.3 were observed, illustrates that a TC without a cirrus-free eye can still have elevated ozone anomalies near the eye (Figure 3.11, left panel). Cirrus or a mixture of cirrus and tall cumulus inhabit the entire central region of the storm on this day (i.e., if there is an eye, it is covered with cirrus). A ring of high ozone levels, sharing a center with Jova, surround

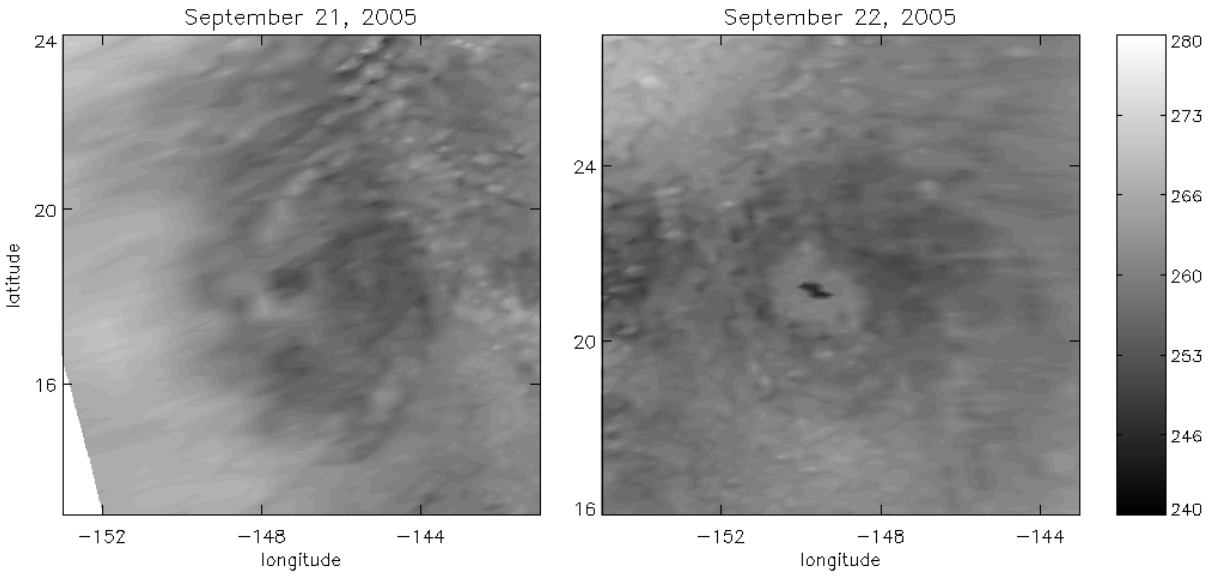


Figure 3.11: Total ozone for Hurricane Jova, about 48 hours (left panel) and 72 hours (right panel) after the data in Fig. 3.3 were collected. Measured by the OMI instrument. Storm center is near 18N, 148W in the left panel and near 21N, 150W in the right panel.

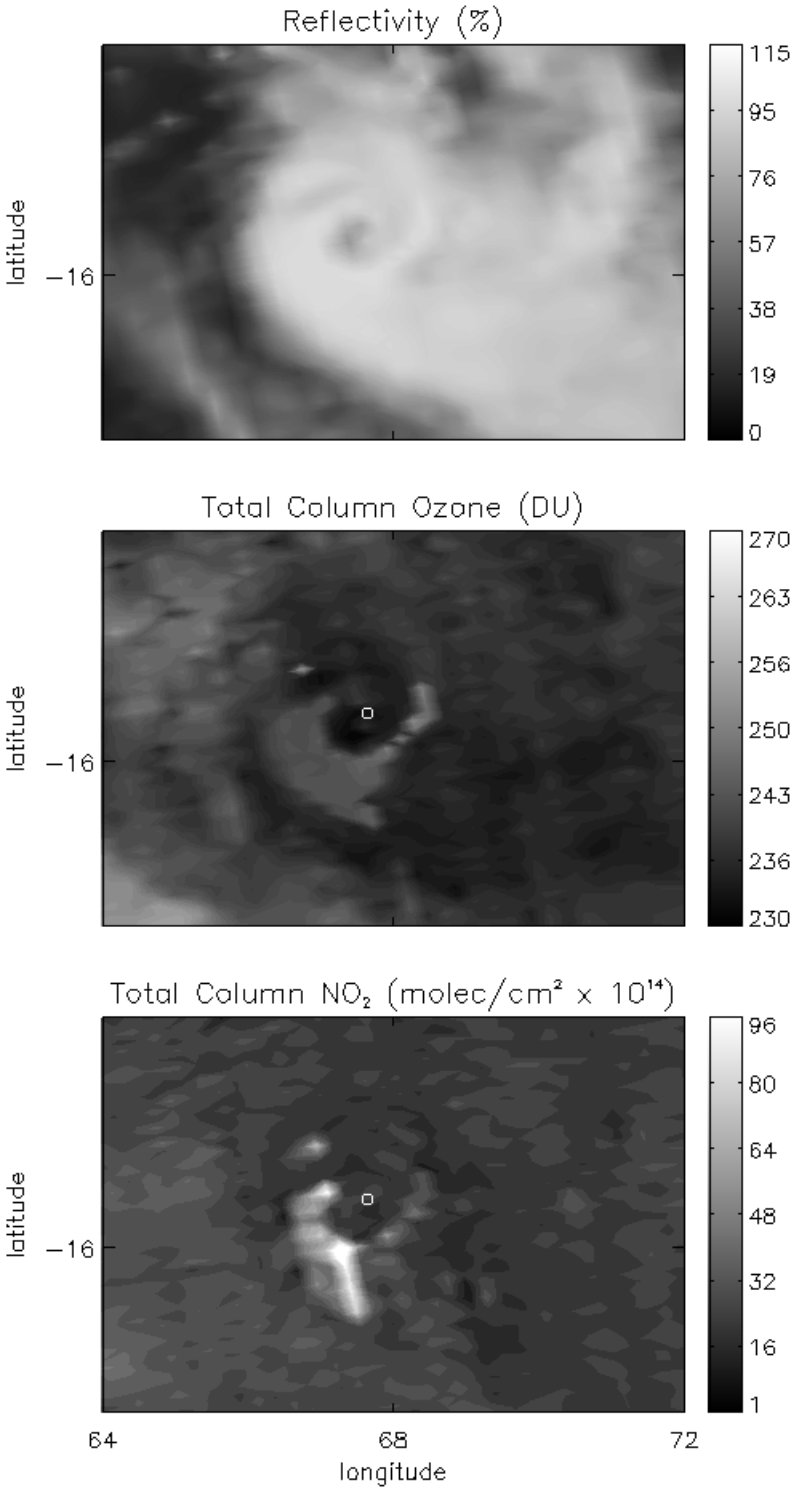


Figure 3.12: As in Fig. 3.6, but for Tropical Cyclone Dora, 9:23 GMT on 1 February, 2007. Dora's eye is depicted by the small white circle in the middle.

an area of low ozone (at 18N, 147.2W). Another example is Tropical Cyclone Dora, shown in Fig. 3.12. Ozone values that are clearly higher than those for the rest of Dora form a band which curves around the center of the storm (middle panel; the eye of the storm is depicted by the small white circle in the middle). This band appears to be part of a rainband. Elevated ozone concentrations appear to be spreading off of the rainband, away from storm center, consistent with upper-level outflow – a feature common to all TCs. The band of high ozone levels does not extend to the eyewall (which is why data for Dora is not included in Tables 3.2 and 3.3; no data for Dora is included in Table 3.4 because there was a gap in Dora's eyewall – the eye was not fully contained). Dora has a cirrus-free eye, but clearly the high ozone levels are not related to any dynamics associated with the eye.

Most of the outflow from the top of a TC's eyewall moves away from storm center. Therefore, if ozone is produced in the eyewall, one would expect somewhat elevated ozone levels outside the eyewall [ozone has a lifetime of roughly 24 days in the upper troposphere (Solomon et al. 2007), so dissipation due to reactions with other chemical species would not be an issue]. This is observed in all of our case studies with high ozone levels in the eyewall. For example, Saomai's eyewall was surrounded by a halo of ozone values that were not as high as those in the eyewall, but generally high compared to those throughout the storm (particularly compared to those in the western half of the storm, see Fig. 3.1, upper right panel). Jova, Ioke (Fig. 3.3, right panel and Fig. 3.4, upper right panel), and Xangsane (not shown) all have halos similar to Saomai's halo. Dora's halo appears to be in its very early stages, when cirrus clouds carrying elevated ozone amounts have recently begun to spread away from a rainband (Fig. 3.12, middle panel). For all of the halos, somewhat elevated ozone amounts apparently haven't had time to spread past the edge of the halo or have become diffuse past the edge.

Note: in Section 3.3, for each storm, we tested whether or not eyewall ozone was significantly different than ozone elsewhere in the cloud shield (Table 3.3). Eyewall ozone was compared to ozone from the rest of the cloud shield, not to ozone from just the halo. It was more appropriate to use ozone from the larger area because upper level outflow winds spread eyewall air outward – i.e., the somewhat high ozone amounts in the halos are likely to be extensions of the very high amounts in the eyewalls. Therefore, comparing eyewall ozone to halo ozone would be comparing eyewall ozone to itself.

### **3.4.3** *High ozone levels in the eye*

Large ozone amounts were measured in much of Ioke's eye and almost all of Damrey's eye. Perhaps ozone was transported into the eye from the eyewall. Stern (2013) and others have shown that some of the outflow from the top of a TC eyewall enters into the eye. Heymsfield et al. (2001) showed convincing evidence that air from the upper portions of the eyewall enters the eye through entrainment by downdrafts along the inside of the eyewall. Perhaps ozone produced by lightning in Ioke's and Damrey's eyewall made its way into the eye through one or both of these mechanisms (cloud particles transported into the eye with the ozone could have evaporated or sublimated, keeping the eye free of cirrus). If so, Damrey's ozone may have had more time to infiltrate the eye – this would explain why large amounts occupy more of Damrey's eye.

When high ozone levels were observed in the eye, Ioke's eyewall contained high ozone levels but Damrey's eyewall did not (Fig. 3.4, upper right and lower left panels, and Fig. 3.6, middle panel). Both storms were at a peak intensity when the elevated ozone in the eye was

measured (Ioke weakened and re-intensified several times; Fig. 3.4 corresponds to the fourth peak). However, TC intensity does not always correlate well with lightning activity (Austin 2010; Sergio Abarca, personal communication, 2014). Thus, lightning activity in Damrey's eyewall could have taken place earlier in the TC lifecycle compared to lightning activity in Ioke's eyewall. If so, perhaps Damrey's lightning produced ozone in the eyewall, then much of the ozone was transported into the eye, then lighting activity (and thus ozone production) in the eyewall stopped, and then air in the eyewall was replaced with air containing lower levels of ozone before the OMI overpass that measured the ozone displayed in Fig. 3.6. Ozone has a lifetime of roughly 22 days throughout the troposphere (Stevenson et al. 2006) and air has a long residence time inside a TC eye (possibly as long as four days, Stern 2013; Newell et al. 1996), so any ozone transported into the eye could persist there long after lightning in the eyewall has ceased and elevated ozone levels have been removed from the eyewall by the upper level outflow.

Considering the above explanation for the excess ozone in Damrey's eye, it makes sense to examine the ozone that was present in Damrey's eyewall prior to the observations in Fig. 3.6. Figure 3.13 shows reflectivity and total ozone for Damrey roughly 24 hours before the ozone in Fig. 3.6 was measured (as noted in Section 3.2.1, OMI measures ozone for each storm only once per day). The eye was capped by cirrus, making it difficult to assess the boundary of the eye. Reflectivity is usually higher for convective clouds compared to cirrus and thus gives an indication of the location of the eyewall and cirrus-capped eye. The circular patch of relatively low reflectivity near the hash marks (shown to aid in comparing the two panels) is a good indication of the location and extent of the eye. The center of Damrey, as determined by navigation, falls within the patch of low reflectivity and the patch is about the same size as the

clearly visible eye the next day. With its proximity to the eye and values indicative of deep convection, the high reflectivity to the south and southeast of the patch indicates the location of part of the eyewall. The location of the high ozone levels in the right panel corresponds well with the area of high reflectivity. Thus it appears there was indeed elevated ozone in the eyewall. Perhaps some of this ozone, and/or eyewall ozone produced over the next 24 hours, was transported into the eye.

Figure 3.14 shows WWLLN lightning strikes that occurred during the two hours prior to the time corresponding to Fig. 3.13 and during the two hours prior to the time corresponding to Fig. 3.6. Many strikes were detected in and near the portion of the eyewall containing elevated ozone prior to the appearance of the elevated ozone (left panel), and just one strike was detected

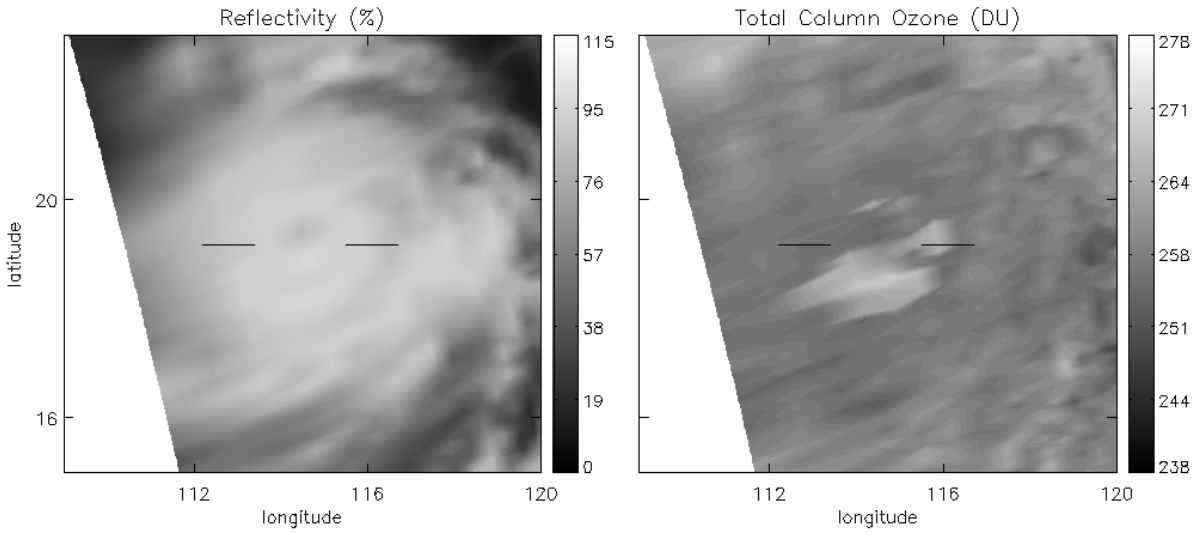


Figure 3.13: Typhoon Damrey, about 24 hours before the data in Fig. 3.6 were collected; (left panel) reflectivity; (right panel) total ozone. Both parameters measured by the OMI instrument. The hash marks near the eye are meant to aid comparison of the two panels.

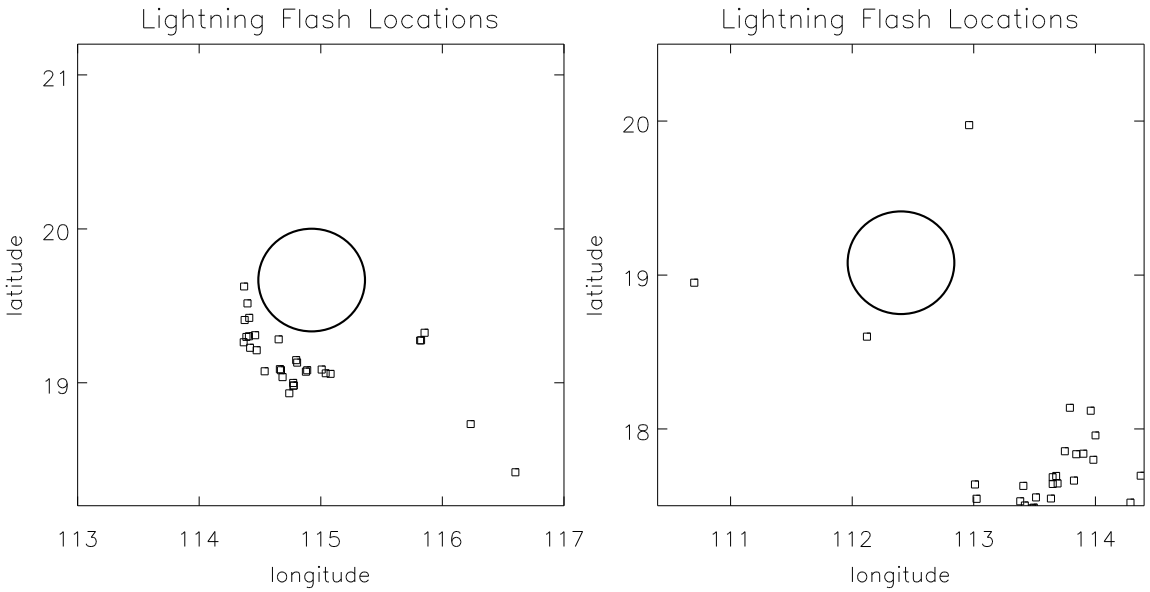


Figure 3.14: Lightning strikes, as detected by the WWLLN, in and near the eyewall of Typhoon Damrey (left panel) during the two hours prior to the measurement of the ozone displayed in Fig. 3.13 and (right panel) during the two hours prior to the measurement of the ozone displayed in Fig. 3.6. Each square represents a strike. The circles represent the boundary of the eye.

in the eyewall prior to elevated ozone appearing inside the eye but not in the eyewall (right panel).

Given the all of the measurements of large eyewall ozone content presented in this study, one might suspect the following as an alternative to the above explanation for Damrey's ozone patterns: Damrey formed concentric eyewalls, then the inner eyewall produced ozone through lightning, then the inner eyewall collapsed, leaving the high ozone content visible in Damrey's eye in Fig. 3.6 (middle panel). Although a definitive determination could not be made, images from satellite microwave sensors (which are unaffected by cirrus clouds and thus can determine eyewall and rainband locations) indicated Damrey did not have concentric eyes before the time corresponding to Fig. 3.6. This, combined with the fact that Damrey's peak intensity was just 41 m/s (it is uncommon for a TC with maximum sustained winds of less than 49 m/s to have

concentric eyewalls; Kuo et al. 2009), leads to the conclusion that Damrey most likely did not form concentric eyewalls prior to the ozone measurements of Fig. 3.6. Furthermore, Damrey's different ozone distribution compared to the other storms cannot be explained by the storms being at different stages of their lifecycle at the time of ozone measurement. Except for Dora, all storms were within nine hours of peak intensity. Damrey and Jova were at precisely the same stage of similar lifecycles. After genesis, both TCs experienced a gradual increase in intensity until spending less than a day at peak intensity, then a gradual decrease in intensity before the dissipation stage. The peak intensity for both storms was nearly the same – 955 hPa for Damrey and 951 hPa for Jova. The OMI overpass time for each storm was closest to the time the storms first reached peak intensity. Despite their similarities, Damrey's eye contained elevated ozone while Jova's eye contained especially low ozone (Tables 3.2 and 3.4).

Some ozone may have entered Saomai's eye prior to the measurements of Fig. 3.1. Although ozone amounts in the eye were substantially lower than those in the eyewall, they were higher than those in the cloud shield (compare Tables 3.2 and 3.3) and those in Saomai's environment (Table 3.4) . Saomai's eye ozone values stand in contrast to those of Jova and Xangsane, both of which had eye values that were very low compared to those in the cloud shield and environment. Perhaps ozone had been transported into the small eye from the eyewall for a relatively short period of time prior to the measurements of Fig. 3.1.

As a test of the hypothesis that large ozone amounts can be transported into the eye from the eyewall, for each TC we examined ozone measured a day after the measurements of elevated eyewall ozone. Unfortunately, Saomai hit land within hours after the ozone in Fig. 3.1 was observed and the eye collapsed. The eyes for Jova, Khanun, and Dora did not show high ozone levels the next day. But on the first day, Jova and Khanun did not exhibit very high ozone levels

in the eyewall (Table 3.3) and Dora's high ozone levels, which appear to be part of a rainband, did not extend to the eyewall (Fig. 3.12, middle panel), so one would not necessarily expect to see substantially elevated ozone in their eyes the next day. More importantly, the eyes for all three storms were capped by thick cirrus the next day, which would have inhibited OMI's ability to measure ozone below (i.e., high ozone concentrations from the eyewall could have been transported into the eye, then the cirrus could have been generated after the eyewall had stopped producing ozone). However, Ioke had a cirrus-free eye the day after high ozone levels were present in the eyewall.

Figure 3.15 shows total ozone for Ioke on 1 September, 2006, roughly 24 hours after the ozone in Fig. 3.4 (upper right and lower left panels) was measured. Ioke was still at typhoon intensity. Ioke's center (near 21N, 164E) was not at OMI's nadir and thus OMI viewed the eye at

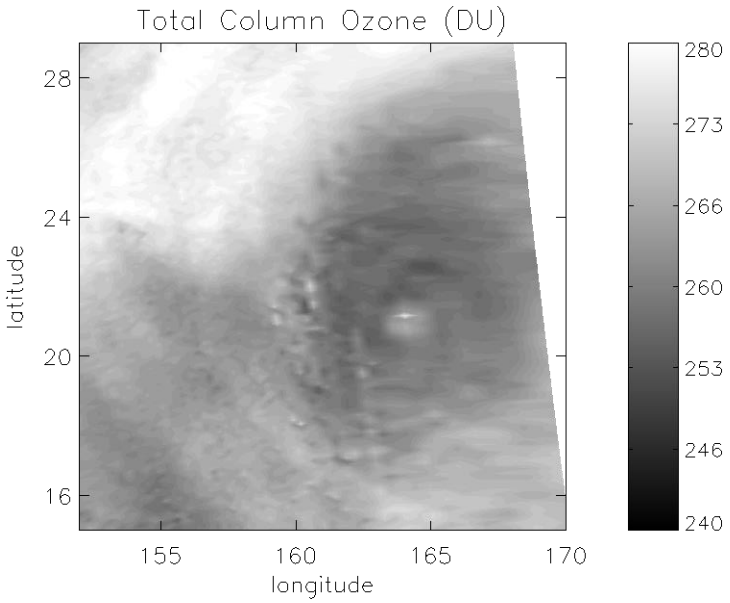


Figure 3.15: Total ozone for Typhoon Ioke, about 24 hours after the data in Fig. 3.4 were collected. Measured by the OMI instrument. Storm center is near 21N, 164E.

a somewhat oblique angle. But effective cloud top pressure and reflectivity measurements similar to those in Fig. 3.2 establish that OMI had a clear view of the low stratus in the eye (not shown). As discussed in Section 3.2.1, most TCs have an eyewall that is sloped at steep angle. The slope of Ioke's eyewall was obviously large enough to allow an obstructed view of the bottom of the eye from OMI's vantage point. OMI FOVs are larger away from nadir than they are at nadir, but apparently an OMI FOV happened to align very well with the large eye and covered little of the eyewall. A large circular region of elevated ozone – larger than the eye – is centered on Ioke's eye. Ozone-rich air occupies the entire eye, in contrast to the day before when parts of the eye contained low ozone amounts (Fig. 3.5). A close-up view of the eye, similar to that in Fig. 3.5, confirms the entire eye contained high ozone levels (not shown). The diameter of the high ozone region is about twice that of the eye, indicating the eyewall still contained high ozone levels. Together, the two days of ozone measurements for Ioke indicate elevated ozone was transported from the eyewall into the eye while ozone production in the eyewall continued throughout the eyewall circumference.

As discussed earlier, at one point, Jova displayed high ozone levels in a ring surrounding storm center while no eye was visible (Fig. 3.11, left panel). The next day, high ozone levels occupied the ring again and also the area within it (Fig. 3.11, right panel; the very dark pixels near Jova's center represent bad data, not low ozone). However, the entire central region was still filled with high cloud tops and it is not clear whether Jova had an eye on this day. It could have been a case of ozone-rich cirrus clouds being expelled by the eyewall and moving over the eye, or a case of an ozone-rich eyewall collapsing and filling the eye region.

### **3.4.4** *Discussion summary*

Collectively, the results and hypotheses discussed above could explain why some previous studies found elevated ozone in TC eyes and others did not. Our primary hypothesis suggests that the elevated eye ozone found in prior studies was produced by lightning in the eyewall and then transported into the eye. In some cases, large amounts of ozone may not yet have been transported into the eye but the high ozone content in the eyewall was mistaken for high ozone content in the eye (partly because of poor viewing angles and low resolution of older satellite instruments). Furthermore, our results suggest that in prior studies, TCs found to have no excess ozone in the eye either had eyewalls that did not produce much lightning, or the ozone measurements in the eye were taken before significant lightning occurred or well after it occurred and after excess ozone in the eye was flushed out. In such cases, the doming effect may have produced eyes with exceptionally low total ozone content.

Heymsfield et al. (2001) found evidence that eyewall outflow into the eye is not continuous, but instead occurs as sporadic events during which large amounts of outflow enter the eye from relatively small portions of the eyewall. If so, then a lack of high ozone levels in TC eyes could be a result of outflow into the eye from portions of the eyewall that did not produce ozone or from portions that did produce ozone, but before or after the production. Similarly, high ozone levels in TC eyes could be a result of outflow into the eye from portions of the eyewall actively producing ozone (or from portions which recently produced ozone).

The very large ozone amounts in the eyes, eyewalls, and even the somewhat large amounts in the halos outside the eyewalls, are especially noteworthy when one considers that any doming taking place in these areas would cause the ozone amounts to tend toward smaller values. If one assumes Jova and Xangsane represent a "basic state" for TCs eyes – a state in

which no eyewall ozone has entered the eye yet – then a "basic state" eye has around 11 DU less ozone than the environment surrounding the TC (Table 3.4). This means the amount of ozone in Damrey's eye would have been around 27.5 DU had eyewall ozone not infiltrated the eye (38.5 DU – 11 DU = 27.5 DU; Table 3.4; Damrey's eye was capped by cirrus on the previous day, so measurement of the amount was inhibited, see Fig. 3.13). Damrey's measured amount of ozone in the eye was 40.6 DU which represents an increase of almost 48% – a very large increase.

### 3.5 Validity of the Results

Tropospheric ozone values herein were calculated from total ozone measurements. As discussed in Section 3.2.1, the OMI algorithm used to determine total ozone estimates the ozone below effective cloud top from climatology. Clouds with effective cloud tops at higher altitudes have more estimated ozone than clouds with effective cloud tops at lower altitudes. Since a TC's eyewall generally has higher effective cloud tops than the rest of the TC, and since estimates can be inaccurate, one may wonder if the large eyewall ozone content presented above is merely an artifact of the eyewalls having larger amounts of estimated below-cloud ozone than elsewhere in the TCs.

Likewise, one may be concerned about the impact of FOVs with high reflectivities. OMI uses reflected sunlight to measure ozone. The total ozone algorithm uses the difference between reflected radiances at two different wavelengths, which mitigates against retrieving a large ozone amount simply as a result of encountering an FOV with high reflectivity. Nevertheless, it is reasonable to suspect that FOVs with high reflectivities could cause problems for the total ozone algorithm which lead to artificially large ozone measurements. And since the rain-laden, tall clouds of an eyewall generally reflect more sunlight than other clouds in a TC, one may wonder

if the large amounts of ozone measured in the eyewalls of the TCs of this study are merely an artifact of high reflectivity.

If the measurements of high ozone levels in the eyewalls are merely an artifact of high cloud tops or strong reflectivity, then elevated ozone should be observed in the eyewall of nearly all mature, intense TCs, because the eyewall of a mature, intense TC almost always contains tall, highly reflective clouds. This is not the case. We examined several mature, intense TCs which, at the time of measurement, had no positive ozone anomalies of note in the eyewall. For example, Fig. 3.16 (right panel) shows total ozone for Jova the day after the measurements of Fig. 3.3 and the day before the measurements shown in the left panel of Fig. 3.11. While Jova had elevated ozone concentrations in the eyewall on the day before and the day after, there is no elevated

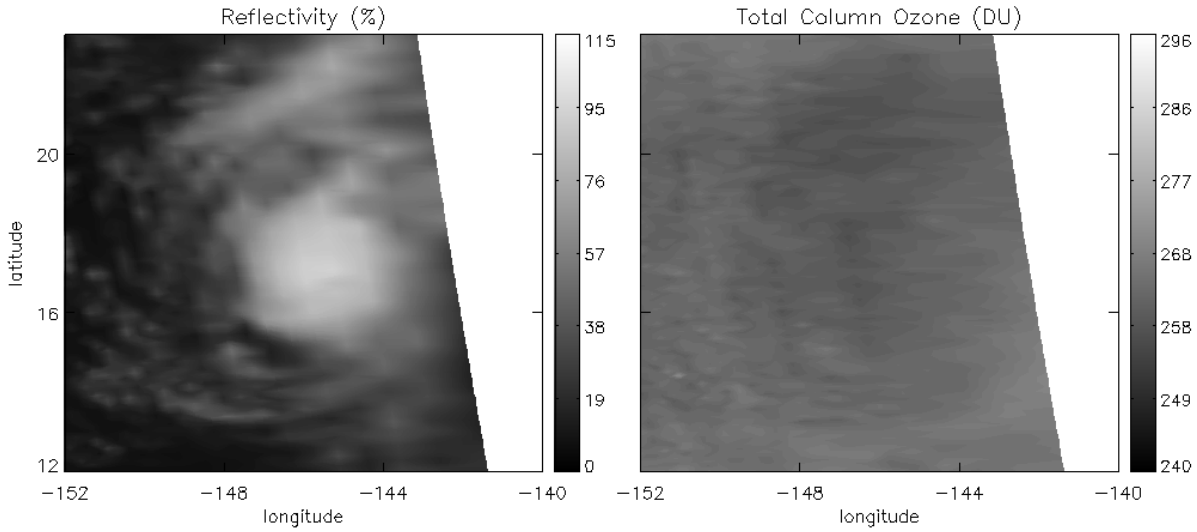


Figure 3.16: As in Fig. 3.3, but roughly 24 hours later.

ozone of note near the eye in Fig. 3.16 (Jova was intense on this day, the central pressure was 957 hPa and the maximum sustained winds were 54 m/s). Cloud top pressures and reflectivities

in and near the eyewall were similar all three days (not shown). Damrey (955 hPa central pressure, 41 m/s maximum sustained winds; Fig. 3.6, middle panel) and Dora (960 hPa central pressure, 39 m/s maximum sustained winds; Fig. 3.12, middle panel) also do not exhibit high ozone concentrations in the eyewall.

More compelling evidence that the ozone observations of this study are not biased comes from plotting total ozone versus reflectivity and versus estimates of ozone below effective cloud top. First, estimates of below-cloud ozone are considered. When comparing FOVs with high effective cloud tops to FOVs with low effective cloud tops, it is worth noting that in FOVs with low tops, less of the troposphere has estimated ozone, but more of the troposphere has measured ozone. For example, an FOV with an effective cloud top of 700 hPa will have ozone estimated between the Earth's surface and 700 hPa. An FOV with an effective cloud top of 400 hPa will have ozone estimated over an additional layer – between 700 and 400 hPa – but the FOV with the 700 hPa effective cloud top will have *measured* ozone for the same layer (700 – 400 hPa; both FOVs will have measured ozone for above 400 hPa).

Figure 3.17 (top panel) shows total ozone for Ioke plotted versus estimated below-cloud ozone. The red dots represent FOVs from the eyewall, the blue dots represent FOVs from the rest of Ioke's cloud shield, and the black X's represent FOVs from everywhere else in Fig. 3.4 (upper right panel). No data from detector 31 are included. When all of the black, blue, and red symbols are considered together, a weak, positive correlation is seen between below-cloud ozone estimates and total ozone. The data representing Ioke's cloud shield (outside of the eyewall) are spread out over a broad range of below-cloud ozone and total ozone values, whereas most of the eyewall data is clustered at high below-cloud values and high total ozone values. At first glance, it may seem the predominance of high below-cloud ozone values in the eyewall biased the total

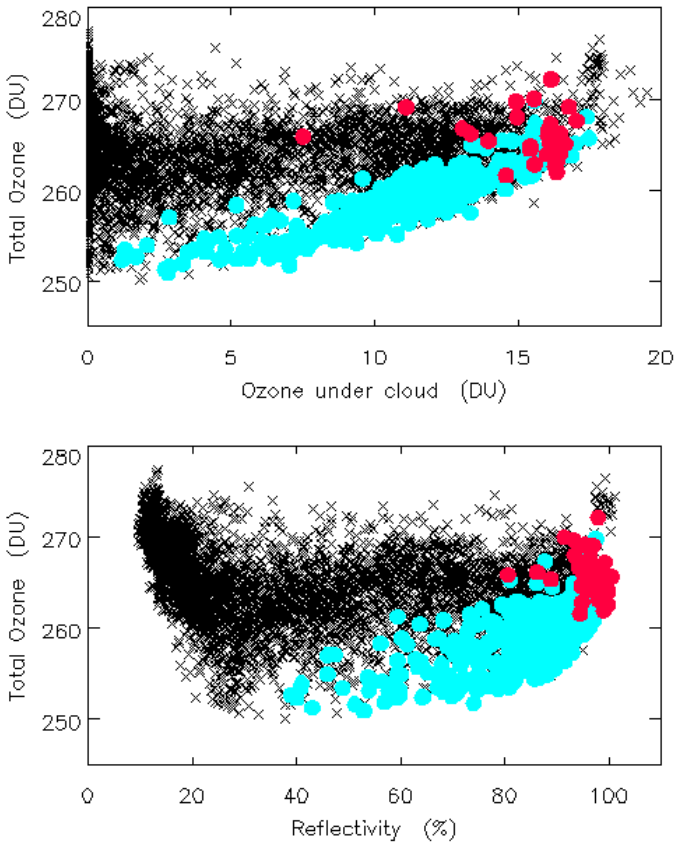


Figure 3.17: Typhoon Ioke; scatterplots correspond to the same date and time for the data in Fig. 3.4; (top) total ozone vs. estimates of below-cloud ozone; (bottom) total ozone vs. reflectivity. Red dots correspond to OMI measurements in the eyewall, blue dots correspond to OMI measurements in the rest of the cloud shield, and black X's correspond to OMI measurements from the rest of the scene shown Fig. 3.4. No data from detector 31 are included.

ozone measurements toward higher values. But the positive below-cloud/total ozone correlation may represent processes that actually took place in nature – for example, locations with more estimated below-cloud ozone are associated with taller convective clouds which are more likely to experience lightning and thus more likely to produce ozone. More importantly, about half of the eyewall FOVs contain total ozone amounts that are greater than the amounts found in any of the FOVs from the rest of the cloud shield that have the same amount of estimated below-cloud

ozone. This demonstrates that the elevated ozone measured in the eyewall is not just a function of the amount of ozone estimated to be below effective cloud top and that atmospheric processes are at work which lead to excess ozone in the eyewall.

Figure 3.17 (bottom panel) shows the same thing as the top panel except total ozone is plotted versus reflectivity. Overall, little or no correlation exists between the two parameters. As expected, the eyewall data is clustered at high reflectivities. The slight positive correlation between reflectivity and total ozone at higher reflectivities could be attributed to processes that actually took place in Ioke (e.g., clouds with very high reflectivities tend to be tall and have much precipitation, both of which are conducive to lightning and thus ozone production), and about half of the values for eyewall total ozone are larger than most or all of the cloud shield values for the same reflectivity (indicating atmospheric processes took place which lead to large ozone amounts in the eyewall).

Scatterplots for Saomai, Jova, and Khanun are similar to Fig. 3.17. Damrey's elevated ozone was inside the eye (Fig. 3.6, middle panel). Because of the low stratus clouds which occupied the eye, there are no concerns that total ozone measurements for the eye were biased by large estimates of below-cloud ozone or by high reflectivity. The estimates of below-cloud ozone for these low clouds were minimal and constituted only a small fraction of the total ozone values. The reflectivity for the clouds in Damrey's eye was relatively low – a mean of 78% for the eye versus a mean of 91% for the eyewall. The robustness of the results for all of the storms supports the hypothesis that lighting can produce large amounts of ozone in a TC eyewall which can then be transported into the eye.

### 3.6 Conclusions

We revisited the issue of high ozone concentrations in TC eyes using observations that are free of many of the limitations of the observations used in previous studies on the same topic. We examined total ozone, as measured by the OMI satellite instrument, corresponding to seven TCs, all of which had cirrus-free eyes. In each case, OMI was almost directly over TC center. This and OMI's relatively small field-of-view allowed OMI to make a more accurate determination of the amount of ozone in the eye and of the locations of anomalous ozone amounts with respect to the eye compared to measurements obtained with a large viewing angle or from older satellites instruments which had larger field-of-views. The OMI data also have advantages compared to aircraft measurements.

For most of the TCs, total ozone levels within the eye were quite low, consistent with the doming effect described by Zou and Wu (2005; deep convection in TCs creates an anomalously high tropopause over the eye). However, anomalously high values of ozone were found in the eyewall and/or rainbands. We hypothesized that deep convection in the eyewall and rainbands generated lightning which catalyzed the formation of ozone. OMI $NO_2$ observations support this hypothesis (lightning also produces $NO_2$). Although limited, WWLLN lightning observations in/near the eyewalls and rainbands also support the hypothesis.

In one of the TCs analyzed, Typhoon Ioke, large amounts of ozone occupied most of the eyewall and also much of the eye (small amounts occupied the rest of the eye). In another TC, Typhoon Damrey, the eyewall did not contain elevated ozone levels but almost the entire eye did. We hypothesized that, for both storms, ozone produced by lightning in the eyewall was transported into the eye by outflow from the tops of eyewall clouds and/or by entrainment from eyewall clouds caused by downdrafts along the inside of the eyewall; in Damrey's case,

lightning/ozone production had ceased by the time of observation and, because of low-level inflow, the ozone-rich air of the eyewall had been replaced by air with less ozone content. In support of these arguments, Damrey's ozone measurements for the previous day showed large ozone amounts in the eyewall and normal amounts in the eye.

The results suggest that TC eyewalls often, but not always, experience lightning which produces high ozone concentrations that can, in turn, be transported into the eye. Our interpretation of the results presents an alternative to the theory that elevated ozone occurs exclusively *within* TC eyes and results either from subsidence of ozone-rich stratospheric air into the eye or a lowered tropopause over the eye. More broadly, while the results herein do not disprove that TC eyes and eyewalls interact with the stratosphere, they suggest that eye/eyewall dynamics are contained within the troposphere.

High ozone concentrations in TC eyes, regardless of the source, could have implications for TC intensity change. In addition to absorbing sunlight, ozone has a strong greenhouse effect, especially when it is in the upper troposphere (Lacis et al. 1990; most of the ozone transport into TC eyes hypothesized herein would take place at upper levels). Perhaps elevated ozone concentrations can warm the eye of a TC through these two heating mechanisms and therefore lower the central pressure (thus increasing the intensity). A thick cirrus canopy over the eye would render the greenhouse effect of ozone irrelevant because the cirrus would be opaque to all longwave radiation from below, creating a "maximum" greenhouse effect. A cirrus canopy would also reduce the amount of solar radiation available for absorption in the eye. Therefore, it may be the case that large amounts of ozone in a TC eye can noticeably influence intensity only when there is no cirrus canopy. Future work will entail modeling efforts to determine if there is a link between eye ozone and intensity and, if so, how much ozone is needed to induce noticeable

intensity changes. If ozone in a TC eye can make a significant impact on intensity, then monitoring TC ozone and, given the results presented in this study, eyewall lightning may aid in intensity predictions, especially when the eye is cirrus-free.

## BIBLIOGRAPHY


Abarca, S. F., K. L. Corbosiero, and T. J. Galarneau Jr., 2010: An evaluation of the Worldwide Lightning Location Network (WWLLN) using the National Lightning Detection Network (NLDN) as ground truth. *J. Geophys. Res.*, **115**, D18206, doi:10.1029/2009JD013411.

Altaratz, O., R. Z. Bar-Or, U. Wollner, and I. Koren, 2013: Relative Humidity and Its Effect on Aerosol Optical Depth in the Vicinity of Convective Clouds. *Environ. Res. Lett.*, **8**, 034025.

Apel, E. C., R. S. Hornbrook, A. J. Hills, N. J. Blake, M. C. Barth, A. Weinheimer, C. Cantrell, S. A. Rutledge, B. Basarab, J. Crawford, G. Diskin, C. R. Homeyer, T. Campos, F. Flocke, A. Fried, D. R. Blake, W. Brune, I. Pollack, J. Peischl, T. Ryerson, P. O. Wennberg, J. D. Crounse, A. Wisthaler, T. Mikoviny, G. Huey, B. Heikes, D. O'Sullivan, and D. D. Riemer, 2015: Upper Tropospheric Ozone Production from Lightning $NO_x$-Impacted Convection: Smoke Ingestion Case Study from the DC3 Campaign. *J. Geophys. Res. Atmos.*, **120**, 2505–2523. doi: 10.1002/2014JD022121.

Austin, M., 2010: "Lightning Observations During Tropical Cyclone Intensity Change: A Composite Study of Spatial and Temporal Relationships". Florida St. Universtiy, Electronic Theses, Treatises and Dissertations. Paper 261.

Carsey, T. P. and H. E. Willoughby, 2005: Ozone Measurements From Eyewall Transects of Two Atlantic Tropical Cyclones. *Mon. Wea. Rev.*, **133**, 166–174.

Chahine, M. T., T. S. Pagano, H. H. Aumann, R. Atlas, C. Barnet, L. Chen, M. Divakarla, E. J. Fetzer, M. Goldberg, C. Gautier, S. Granger, F. W. Irion, R. Kakar, E. Kalnay, B. H. Lambrigtsen, S. Y. Lee, J. Le Marshall, W. McMillan, L. McMillin, E. T. Olsen, H.

Revercomb , P. Rosenkranz, W. L. Smith, D. Staelin, L. L. Strow, J. Susskind, D. Tobin and W. Wolf, 2006: The Atmospheric Infrared Sounder (AIRS): Improving Weather Forecasting And Providing New Insights Into Climate. *Bulletin of the American Meteorological Society*, **87**, 891–894.

Chang-Hoi, H., M. Chou, M. Suarez, and K. Lau, 1998: Effect of ice cloud on GCM climate simulations, *GRL*, **25**, 71-74, 10.1029/97GL03356

Chen, Y., 1985: Tropical Squall Lines over the Eastern Atlantic during GATE. *Mon. Wea. Rev.*, **113**, 2015 – 2022.

DeCaria, A. J., K. E. Pickering, G. L. Stenchikov, and L. E. Ott, 2005: Lightning-Generated NOx and its Impact on Tropospheric Ozone Production: A Three-Dimensional Modeling Study of a Stratosphere-Troposphere Experiment: Radiation, Aerosols, and Ozone (STERAO-A) Thunderstorm. *J. Geophys. Res.*, **110**, doi:10.1029/2004JD005556.

DeMaria, M., J. A. Knaff, B. H. Connell, 2001: A Tropical Cyclone Genesis Parameter for the Tropical Atlantic. *Wea. Forecasting*, **16**, 219–233.

Dunion, J. P., 2011: Rewriting the Climatology of the Tropical North Atlantic and Caribbean Sea Atmosphere. *J. Climate*, **24** (3), 893-908.

Dunion, J. P., and C. S. Velden, 2004: The Impact of the Saharan Air Layer on Atlantic Tropical Cyclone Activity. *Bull. Am. Meteorol. Soc.*, **85**, 353-365.

Dunkerton, T. J., M. Montgomery, and Z. Wang, 2008: Tropical Cyclogenesis in a Tropical Wave Critical Layer: Easterly Waves. *Atmos. Chem. Phys.*, **8**, 11149–11292.

Emanuel, K. A., 1994: Atmospheric convection. *Oxford University Press*, 580pp.

Emanuel, K. A., and D. S. Nolan, 2004: Tropical cyclone activity and global climate. Preprints,

*26th Conf. on Hurricanes and Tropical Meteorology*, Miami, FL, Amer. Meteor. Soc., 240–241.

Fu, Y. F., T. Xian, D. R. Lü, G. Liu, Z. Heng, L. Sun, Q. Liu, Y. Wang, and Y. Yang, 2013: Ozone Vertical Variations During a Typhoon Derived from the OMI Observations and Reanalysis Data. *Chin Sci Bull*, **58**, 3890–3894, doi: 10.1007/s11434-013-6024-7

Gray, W. M., 1968: Global View Of The Origin Of Tropical Disturbances And Storms. *Mon. Wea. Rev.*, **96**, 669–700.

Gray, W. M., 1979: Hurricanes: Their formation, structure and likely role in the tropical circulation. *Meteorology over the Tropical Oceans*, D. B. Shaw, Ed., Royal Meteorological Society, 155–218.

Gray, W. M., 1998: The Formation of Tropical Cyclones. *Meteorol. Atmos. Phys.*, **67**, 37-69.

Gray, W. M., J. D. Scheaffer, and J. A. Knaff, 1992: Influence of the stratospheric QBO on ENSO variability. *J. Meteor. Soc. Japan*, **70,** 975–995.

Hendricks, E. A., M. T. Montgomery, and C. A. Davis, 2004: The Role of "Vortical" Hot Towers in the Formation of Tropical Cyclone Diana (1984). *J. Atmos. Sci.*, **61**, 1209–1232.

Heymsfield, G. M., J. B. Halverson, J. Simpson, L. Tian, and T. P. Bui, 2001: ER-2 Doppler Radar Investigations of the Eyewall of Hurricane Bonnie during the Convection and Moisture Experiment-3. *J. Appl. Meteor.*, **40**, 1310–1330.

Hicks, E., C. Pontikis and E. Williams, 2008 : The influence of desertic aerosols on tropical cyclones, *28th Conference on Tropical Meteorology and Hurricanes*, Orlando, Florida, Amer. Meteor. Soc.

Houze, R. A., 2010: Clouds in Tropical Cyclones. *Mon. Wea. Rev.*, **138**, 293-344.

Huntrieser, H., H. Schlager, C. Feigl, *and* H. Höller, 1998: Transport and Production of $NO_X$ in Electrified Thunderstorms: Survey of Previous Studies and New Observations at Midlatitudes. *J. Geophys. Res.*, **103**, D21, 28247–28264, doi:10.1029/98JD02353.

Järvinen, E., M. Schnaiter, G. Mioche, O. Jourdan, V.N. Shcherbakov, A. Costa, A. Afchine, M. Krämer, F. Heidelberg, T. Jurkat, C. Voigt, H. Schlager, L. Nichman, M. Gallagher, E. Hirst, C. Schmitt, A. Bansemer, A. Heymsfield, P. Lawson, U. Tricoli, K. Pfeilsticker, P. Vochezer, O. Möhler, and T. Leisner, 2016: Quasi-Spherical Ice in Convective Clouds. *J. Atmos. Sci.*, **73**, 3885–3910, https://doi.org/10.1175/JAS-D-15-0365.1

Joiner, J., A. Vasilkov, K. Yang, and P. K. Bhartia, 2006: Observations Over Hurricanes from the Ozone Monitoring Instrument. *Geophys. Res. Lett.*, **33**, L06807, doi:10.1029/2005GL025592.

Joiner, J., A. P. Vasilkov, P. Gupta, P. K. Bhartia, P. Veefkind, M. Sneep, J. de Haan, I. Polonsky, and R. Spurr, 2012: Fast Simulators for Satellite Cloud Optical Centroid Pressure Retrievals; Evaluation of OMI Cloud Retrievals. *Atmos. Meas. Tech.*, **5**, 529-545, doi:10.5194/amt-5-529-2012.

Knapp, K. R., M. C. Kruk, D. H. Levinson, H. J. Diamond, and C. J. Neumann, 2010: The International Best Track Archive for Climate Stewardship (IBTrACS): Unifying tropical cyclone best track data. *BAMS*, **91**, 363-376. doi:10.1175/2009BAMS2755.1

Krall, G. M., and W. R. Cotton, 2012 : Potential indirect effects of aerosol on tropical cyclone intensity: convective fluxes and cold-pool activity. *Atmos. Chem. Phys. Discuss.*, **12**, 351-385.

Kuo, H., C. Chang, Y. Yang, H. Jiang, 2009: Western North Pacific Typhoons with Concentric Eyewalls. *Mon. Wea. Rev.*, **137**, 3758–3770.

Lacis, A. A., D. J. Wuebbles, and J. A. Logan, 1990: Radiative Forcing of Climate by Changes in the Vertical Distribution of Ozone. *J. Geophys. Res.*, **95**, 9971-9981, doi:10.1029/JD095iD07p09971

Levelt, P. F., G. H. J. van den Oord, M. R. Dobber, A. Mälkki, H. Visser, J. de Vries, P. Stammes, J. O. V. Lundell, and H. Saari, 2006: The Ozone Monitoring Instrument. *IEEE Transactions On Geoscience And Remote Sensing*, **44**, 5, 1093-1101.

Liu, J. and Z. Li, 2014: Estimation of Cloud Condensation Nuclei Concentration from Aerosol Optical Quantities: Influential Factors and Uncertainties. *Atmos. Chem. Phys.*, **14**, 471-483.

Lynn, B. and A. Khain, 2010: Effects of aerosols on the tropical cyclone genesis as seen from simulations using Spectral Bin Microphysics Model (the HAMP contribution). *29th Conference on Hurricanes and Tropical Meteorology*, **Tucson, Arizona**, Amer. Meteor. Soc.

Masunaga, H. and Z. J. Luo, 2016: Convective and large-scale mass flux profiles over tropical oceans determined from synergistic analysis of a suite of satellite observations. *JGR Atmos.*, **121**, doi:10.1002/2016JD024753.

McTaggaert-Cowan, G., D. Deane, L. F. Bosart, C. A. Davis, and T. J. Galarneau Jr., 2008: Climatology of tropical cyclogenesis in the North Atlantic (1948–2004). *Mon. Wea. Rev.*, **136**, 1284–1304.

Minschwaner, K., L. E. Kalnajs, M. K. Dubey, L. M. Avallone, P. C. Sawaengphokai, H. E. Edens, and W. P. Winn, 2008: Observation of Enhanced Ozone in an Electrically Active Storm Over Socorro, NM: Implications for Ozone Production From Corona Discharges. *J. Geophys. Res.*, **113**, D17208, doi:10.1029/2007JD009500.

Mooney, P. A., F. J. Mulligan, and R. Fealy, 2011: Comparison of ERA-40, ERA-Interim and NCEP/NCAR reanalysis data with observed surface air temperatures over Ireland. *International Journal of Climatology*, **31**, 4, 545-557.

Newell, R. E., et al., 1996: Atmospheric Sampling of Supertyphoon Mireille With NASA DC-8 Aircraft on September 27, 1991, During PEM-West A. *J. Geophys. Res.*, **101**, D1, 1853–1871, doi:10.1029/95JD01374.

Orville, R. E., 1967: Ozone Production During Thunderstorms, Measured by the Absorption of Ultraviolet Radiation from Lightning. *J. Geophys. Res.*, **72**(14), 3557–3561, doi:10.1029/JZ072i014p03557.

Ott, L. E., K. E. Pickering, G. L. Stenchikov, H. Huntrieser, and U. Schumann, 2007: Effects of Lightning $NO_x$ Production During the 21 July European Lightning Nitrogen Oxides Project Storm Studied with a Three-Dimensional Cloud-Scale Chemical Transport Model. *J. Geophys. Res.*, **112**, D05307, doi:10.1029/2006JD007365.

Palmen, E., 1948: On the formation and structure of tropical cyclones. *Geophysics*, **3,** 26–38.

Penn, S., 1965: Ozone and Temperature Structure in a Hurricane. *J. Appl. Meteorol.*, **4**, 212–216.

Penn, S., 1966: Temperature and Ozone Variations Near Tropopause Level Over Hurricane Isbell October 1964. *J. Appl. Meteorol.*, **5**, 407–410.

Pickering, K. E., A. M. Thompson, J. R. Scala, W.-K. Tao, R. R. Dickerson, and J. Simpson, 1992: Free Tropospheric Ozone Production Following Entrainment of Urban Plumes Into Deep Convection. *J. Geophys. Res.*, **97**, 17985-18000.

Pickering, K. E., et al., 1996: Convective Transport of Biomass Burning Emissions Over Brazil During TRACE A. *J. Geophys. Res.*, **101**(D19), 23993–24012, doi:10.1029/96JD00346.

Platnick, S., 2000: Vertical photon transport in cloud remote sensing problems. *J. Geophys.*

*Res.*, **105**(D18), 22919–22935, doi:10.1029/2000JD900333.

Prather, M., et al., 2001: Atmospheric Chemistry and Greenhouse Gases, in Climate Change 2001: The Scientific Basis. Contribution of Working Group I to the Third Assessment Report of the Intergovernmental Panel on Climate Change, edited by J. T. Houghton et al., Cambridge Univ. Press, Cambridge, U. K., 239–287.

Price, C., M. Asfur, and Y. Yair, 2009: Maximum hurricane intensity preceded by increase in lightning frequency. *Nat. Geosci.*, **2**, 329–332, doi:10.1038/NGEO477.

Ravetta, F. and G. Ancellet, 2000: Identification of Dynamical Processes at the Tropopause During the Decay of a Cutoff Low Using High-Resolution Airborne Lidar Ozone Measurements. *Mon. Wea. Rev.*, **128**, 3252–3267.

Rodgers, E. B., J. Stout, J. Steranka, and S. Chang, 1990: Tropical Cyclone-Upper Atmospheric Interaction as Inferred From Satellite Total Ozone Observations. *J. Appl. Meteorol.*, **29**, 934–954.

Rosenfeld, D., U. Lohmann, G. B. Raga, C. D. O'Dowd, M. Kulmala, S. Fuzzi, A. Reissell, and M. O. Andreae, 2008: Flood or Drought: How Do Aerosols Affect Precipitation? *Science*, 1309-1313.

Rosenfeld, D., W. L. Woodley, A. Khain, W. R. Cotton, G. Carrió, I. Ginis, and J. H. Golden, 2012: Aerosol Effects on Microstructure and Intensity of Tropical Cyclones. *Bull. Amer. Meteor. Soc.*, **93**, 987-1001.

Schmitt, C.G., M. Schnaiter, A.J. Heymsfield, P. Yang, E. Hirst, and A. Bansemer, 2016: The Microphysical Properties of Small Ice Particles Measured by the Small Ice Detector-3 Probe during the MACPEX Field Campaign. *J. Atmos. Sci.*, **73**, 4775–4791, https://doi.org/10.1175/JAS-D-16-0126.1

Schumann, U. and H. Huntrieser, 2007: The global lightning-induced nitrogen oxides source. *Atmos. Chem. Phys.*, **7**, 3823-3907, doi:10.5194/acp-7-3823-2007.

Seinfeld, J. H. and S. N. Pandis, 2006: *Atmospheric Chemistry and Physics: From Air Pollution to Climate Change*. John Wiley and Sons, Inc., Hoboken, NJ.

Shu, S. and L. Wu, 2009: Analysis of the influence of Saharan air layer on tropical cyclone intensity using AIRS/Aqua data. *Geophysical Research Letters*, **36**, L09809, 5pp.

Shupe, M. D., T. Uttal, S. Y. Matrosov, and A. S. Frisch, 2001: Cloud Water Contents and Hydrometeor Sizes During the FIRE-Arctic Clouds Experiment. *JGR*, **106**, No. D14, 15,015–15,028.

Solomon, S., D. Qin, M. Manning, Z. Chen, M. Marquis, K. B. Averyt, M. Tignor, and H. L. Miller (eds.), 2007: Contribution of Working Group I to the Fourth Assessment Report of the Intergovernmental Panel on Climate Change. Cambridge University Press, Cambridge, United Kingdom and New York, NY, USA, Ch. 7.4.4.

Stevenson, D. S., et al., 2006: Multimodel Ensemble Simulations of Present-Day and Near-Future Tropospheric Ozone. *J. Geophys. Res.*, **111**, D08301, doi:10.1029/2005JD006338.

Smith, R. K. and M. T. Montgomery, 2011: Observations of the convective environment in developing and non-developing tropical disturbances. *Q. J. R. Meteorol. Soc.* **137**, 1–18.

Tao, W.-K., X. Li, A. Khain, T. Matsui, S. Lang, and J. Simpson , 2007: Role of Atmospheric Aerosol Concentration on Deep Convective Precipitation: Cloud-resolving Model Simulations. *J. Geophys. Res.*, **112**, D24S18, doi:10.1029/2007JD008728.

Tuleya, R. E. and Y. Kurihara, 1981: Numerical study of the effects of environmental flow on tropical storm genesis. *Mon. Wea. Rev.*, **109**, (12), 2487-2506.

Thompson A. M., W.-K. Tao, K. E. Pickering, J. R. Scala, and J. Simpson, 1997:

Tropical deep convection and ozone formation, *Bull. Am. Meteorol. Sot.*, **78**, 1043-1054.

van Diedenhoven, B., A. M. Fridlind, B. Cairns, A. S. Ackerman, and J. E. Yorks, 2016: Vertical Variation of Ice Particle Size in Convective Cloud Tops. *Geophys. Res. Lett.*, **43**,4586–4593, doi:10.1002/2016GL068548

Vasilkov, A. P., J. Joiner, K. Yang, and P. K. Bhartia, 2004: Improving Total Column Ozone Retrievals by Using Cloud Pressures Derived From Raman Scattering in the UV. *Geophys. Res. Lett.*, **31**, L20109, doi:10.1029/2004GL020603.

Vasilkov, A. P., J. Joiner, R. Spurr, P. K. Bhartia, P. F. Levelt, and G. Stephens, 2008: Evaluation of the OMI Cloud Pressures Derived From Rotational Raman Scattering by Comparisons With Satellite Data and Radiative Transfer Simulations. *J. Geophys. Res.*, **113**, D15S19, doi:10.1029/2007JD008689.

Wu, L., H. Su, R. G. Fovell, B. Wang, J. T. Shen, B. H. Kahn, S. M. Hristova-Veleva, B. H. Lambrigtsen, E. J. Fetzer, and J. H. Jiang, 2012: Relationship of environmental relative humidity with North Atlantic tropical cyclone intensity and intensification rate. *Geophys. Res. Lett.*, **39**, L20809, doi:10.1029/2012GL053546.

Yoon, S. and J. Kim, 2006: Influences of Relative Humidity on Aerosol Optical Properties and Aerosol Radiative Forcing During ACE-Asia. *Atmos. Environ.*, **40** (23), 4328-4338.

Zehr, R. M., 1992: Tropical cyclogenesis in the western north Pacific. *NOAA Tech. Rep. NESDIS 61*, 181 pp.

Zhang, J. A., R. F. Rogers, D. S. Nolan, and F. D. Marks Jr., 2011: On the Characteristic Height Scales of the Hurricane Boundary Layer. *Mon. Wea. Rev.*, **139**, 2523–2535.

Zou, X. and Y. Wu, 2005: On the Relationship Between Total Ozone Mapping Spectrometer (TOMS) Ozone and Hurricanes. *J. Geophys. Res.*, **110**, D06109, doi:10.1029/2004JD005019